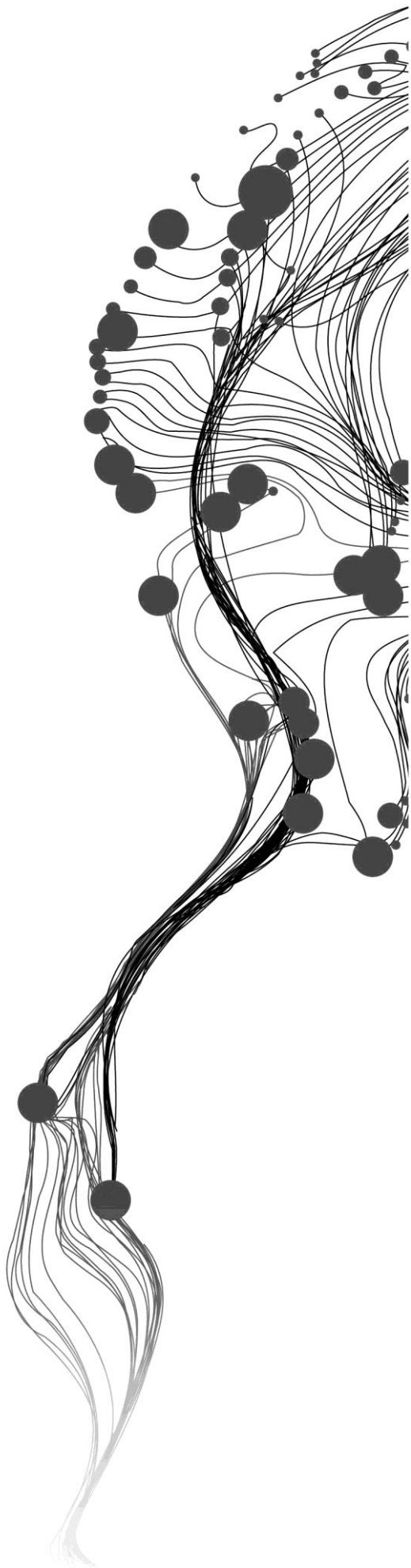


**INVESTIGATING SINGO  
GRANITE ANOMALY IN KIBOGA,  
CENTRAL UGANDA, USING  
AEROMAGNETIC AND REMOTE  
SENSING DATA**

ALADE OMOTOLA OLUFADEKEMI  
February, 2011

SUPERVISORS:  
DR.T.WOLDAI  
DR.M.F.NOOMEN



# **INVESTIGATING SINGO GRANITE ANOMALY IN KIBOGA, CENTRAL UGANDA, USING AEROMAGNETIC AND REMOTE SENSING DATA**

ALADE OMOTOLA OLUFADEKEMI

Enschede, The Netherlands, February, 2011

Thesis submitted to the Faculty of Geo-Information Science and Earth  
Observation of the University of Twente in partial fulfilment of the  
requirements for the degree of Master of Science in Geo-information Science  
and Earth Observation.

Specialization: Applied Earth Sciences

SUPERVISORS:

DR.T.TSEHAIE WOLDAI

DR.M.F.MARLEEN NOOMEN

THESIS ASSESSMENT BOARD:

Prof. Dr. F.D. van der Meer (Chair)

Dr. P.M. van Dijk (External Examiner, ITC, University of Twente)

#### DISCLAIMER

This document describes work undertaken as part of a programme of study at the Faculty of Geo-Information Science and Earth Observation of the University of Twente. All views and opinions expressed therein remain the sole responsibility of the author, and do not necessarily represent those of the Faculty.

## ABSTRACT

The use of aeromagnetic survey as geophysical exploration technique has tremendously grown over the past few years. The study involves analysis of Aeromagnetic data and other remote sensing data sets in collaboration with field work to study the Singo granite in Kiboga area, Central Uganda. Geological mapping and magnetic susceptibility measurements were acquired during the field work. Aeromagnetic analysis was performed using Oasis Montaj software and several filtering techniques were executed i.e. analytical signal, vertical derivative, horizontal derivative, tilt derivative and 3D Euler deconvolution was used to characterize the magnetic sources. In addition, along three geological cross sections Potent software was used to model the Singo granite and its physical properties.

The magnetic susceptibility measured along several walking traverses using a Kappa meter showed highly variable readings (0.01, 0.05, 0.23 and 1.19); similarly the measurements obtained in the areas covered by Singo granite have huge variations ranging from 0.03 to 5.72. However, on map deduced from aeromagnetic survey, areas covered by the metasediments are reflected by relatively low magnetic anomaly that is laterally extensive, the trace of outermost margin of the Singo granite is expressed by high frequency magnetic sources. The results from the SRTM DEM and Aster show that the drainage pattern is structurally controlled and filtering techniques (Oasis Montaj) indicate that NW-SE dykes are the dominant in the study area and they cut all the geological formations. In addition, the presence of echelon shaped deflections is an indication that this area is tectonically active.

3D Euler deconvolution results show magnetic sources as either linear features or clustered. The linear sources are oriented in either NW-SE or NE-SW, with NW-SE being widely distributed. Most of these magnetic sources are confined in the zone between 300-400 m but some at the borders of the Singo granite are localized within shallow depths (100-200m). Further, the sub-parallel NE-SE is cut by the NW-SE linear structures, indicating a strong persistence of the NW-SE linear structures. Geologically, the NE-SW marks the Singo granite which majorly has no sources except along its outer margins and where it is cut through by the NW-SE linear structures. This indicates that the granite intrusion is much older than the faulting mechanism. The margin along the Singo granite possibly indicates lateritic material (alteration products i.e. tourmaline and hematite) marking the contact between the Singo granite and the host rock. The clustered but isolated magnetic sources are rather deep seated (500m) and have a rather poorly defined E-W trend. From 2D modelling in Potent, it is clear that the magnetic susceptibility of the metasediments is very low ranging from 0 to and 0.0005 whereas that of the granite is relatively slightly higher stable 0.003. These susceptibility values have the same order of magnitude for all the three profiles. From the potent, the source of magnetic anomaly at the periphery was determined.

Keywords: Singo granite, aeromagnetic data, magnetic susceptibility, 3D Euler deconvolution, modelling.

## ACKNOWLEDGEMENTS

I am grateful to God Almighty for his grace, mercy, strength, power, sustenance and for the completion of my MSC program. I wish to extend my sincere thanks to the Dutch Government for providing financial assistance through an NFP fellowship.

My appreciation goes to my supervisors, Dr T. Woldai and Dr M.F Noomen. Dr M.F. Noomen for her assistance and guidance in geophysical aspect of the study. I also want to thank Drs. T.M. Loran, the Applied Earth Science (AES) Course Director for his efforts in ensuring a successful running of the MSc program. Many thanks also to Drs. Boudewijn de Smeth for his advice and encouragement during the study period at ITC. I also thank Dr. F.J.A van Ruitenbeek and Dr. E.J.M Carranza of Earth Resources Exploration stream for their valuable instructions during this program and Dr. M. Mark Van der Meijde.

I would like to thank Dr. Nigel Stack from Fugro and Dr. Sally Barrit who works in Geowitch who helped with getting the high resolution aeromagnetic imagery for this research and also, i thank the department of Geological Survey and Mines (DGSM) for their permission to use the aeromagnetic for my research.

I also appreciate Mr Zack Kuria for his advice during this research work. I would like to express my gratitude towards all people who have contributed in various ways to the successful completion of this work in ITC.

My special appreciation goes to my husband, Mr Charles Durojaye for his love, patient and encouragement during my MSc study. I also appreciate my parents Mr. & Mrs. Alade, my in-laws and my siblings for their prayers and encouragements during my stay in the Netherlands.

Thanks to my family friend in Enschede, Mr Gregory Ajibolade and Mrs Christine Ajibolade for their warmth encouragement all through my stay in Enschede for the M.Sc study. You really made Enschede a home for me.

All my fellow students in ITC especially Applied earth Sciences and all my instructors who contributed in one way or the other to my stay in ITC, I say thank you. I am also appreciating my apartment mate Mrs. Ayomiposi Grace Oluwadebi for her encouragement and companionship.

# TABLE OF CONTENTS

---

1.	INTRODUCTION.....	1
1.1.	Background.....	1
1.2.	Study area.....	1
1.3.	Previous work.....	2
1.4.	Problem statement.....	3
1.5.	Objective of the research.....	4
1.5.1.	General objectives.....	4
1.5.2.	Specific objectives.....	4
1.6.	Research questions.....	4
1.7.	Thesis structure.....	4
2.	LITERATURE REVIEW.....	5
2.1.	Regional geology.....	5
2.1.1.	Basement complex.....	6
2.1.2.	Nyanzian Sequence.....	6
2.1.3.	Lower Proterozoic mobile belt.....	7
2.1.4.	Middle-upper Proterozoic Mobile belt.....	7
2.1.5.	Upper Proterozoic sediments.....	8
2.2.	Geology of Kiboga Area.....	8
2.2.1.	General geology of the area.....	8
2.2.2.	The Granitic Gneisses (basement complex).....	9
2.2.3.	The Buganda series.....	9
2.2.4.	The Kiye Schists.....	10
2.2.5.	The Singo series.....	10
2.2.6.	The Mityana series.....	10
2.2.7.	The Singo granite.....	10
2.2.8.	The Mubende Batholiths.....	12
3.	MAGNETIC PETROPHYSICS.....	13
3.1.	Airborne magnetic survey.....	13
3.2.	Rock magnetism.....	13
3.3.	Influence of metamorphism.....	13
3.4.	Magnetic susceptibility.....	14
3.5.	Filtering of aeromagnetic data.....	15
3.6.	Field inversion.....	15
4.	DATA SETS AND METHODOLOGY.....	17
4.1.	Description of data sets.....	17
4.1.1.	Geological map and mineral occurrence point.....	17
4.1.2.	Remote sensing data.....	17
4.1.3.	Geophysical data.....	17
4.2.	Software used.....	18
4.3.	Methodology.....	18
4.3.1.	Pre-field work.....	18
4.3.2.	Field work.....	18
4.3.3.	Post-field work.....	19
4.4.	3D Euler deconvolution.....	19
4.4.1.	Depth results.....	19
5.	INTERPRETATION & INTEGRATION.....	21

5.1.	Field work .....	21
5.2.	Aeromagnetic Data .....	23
5.2.1.	Total magnetic intensity.....	23
5.2.2.	Analytical signal.....	23
5.2.3.	Tilt Derivative .....	24
5.2.4.	Horizontal derivative of tilt.....	25
5.2.5.	Vertical derivative .....	26
5.2.6.	3D Euler deconvolution (Depth result).....	27
5.3.	Integration of Dataset.....	28
6.	MODELLING OF AEROMAGNETIC ANOMALY .....	29
6.1.	Forward and inversion modelling.....	29
6.2.	Methodology .....	29
6.3.	Conceptual geological model.....	30
7.	DISCUSSION OF RESULTS AND CONCLUSION.....	35
7.1.	Discussion.....	35
7.1.1.	To establish magnetic susceptibility contrast between granite and its surrounding rocks.....	35
7.1.2.	To determine the depth to the source of magnetic anomaly.....	35
7.1.3.	To model the magnetic anomaly integrating surface and subsurface structures .....	36
7.1.4.	To establish the relationship between the magnetic anomaly, the geological structures and its associated mineralization .....	37
7.2.	Conclusion .....	37
7.3.	Research Limitation .....	37
7.4.	Recommendation .....	37

## LIST OF FIGURES

---

Figure 1.1: The location of the study area. ....	2
Figure 1.2: The TMI map showing the Singo granite with variation in magnetic susceptibility.....	3
Figure 2.1: Simplified diagram showing isotopic age (bars) of Precambrian tectono-thermal veins in Uganda (Leggo, 1974).....	5
Figure 2.2: Geology of Uganda simplified after (Gabert, 1990) .....	6
Figure 2.3: Probable geological sequence of Uganda after (Johnson & Williams, 1961).....	8
Figure 2.4: Geological map of Kiboga area after (Johnson & Williams, 1961) .....	9
Figure 2.5: Simplified geological map of Uganda showing the location of Singo granite and some structural features (modified after MacDonald (1966). ....	11
Figure 3.1: Susceptibility ranges of common rock types (from Clark & Emerson 1991).....	14
Figure 3.2: Schematic method of Euler deconvolution. Input data; dx, dy and dz are x,y and z derivative grids respectively of the input and mag = magnetic field input grid (from Kuttikul 1995). ....	15
Figure 4.1: Flow chart showing the research methodology .....	19
Figure 4.2: Steps followed for 3D Euler deconvolution .....	20
Figure 5.1a: Cross section A-B and visited points displayed on geological map.....	21
Figure 5.1b: Geological cross section of profile A-B, 5.1c stratigraphy column for profile A-B.....	22
Figure 5.2: (a) Box plot showing the different values of magnetic susceptibilities of the three lithologies; (b) Histogram showing variation in the five lithologies. ....	22
Figure 5.3: Magnetic susceptibilities values for weathered and unweathered granite.....	22
Figure 5.4: Diagram of Total magnetic intensity .....	23
Figure 5.5: Resulting map from analytical signal .....	24
Figure 5.6: Diagram of tilt derivative.....	25
Figure 5.7: Diagram of Horizontal derivative of tilt .....	26
Figure 5.8: Diagram of Vertical derivative.....	26
Figure 5.9: The Depth result from 3D Euler Deconvolution.....	27
Figure 5.10: (a) Surface structures from SRTM DEM; (b) Integration of datasets .....	28
Figure 6.1: (a) Geosoft V2 Grid Header file showing the analytical signal used for the modelling; (b) Analytical signal, the horizontal axis is the distance in metre, while the vertical axis is the observed analytical signal in nanotesla .....	30
Figure 6.2: Figure showing the profile lines used for the modelling.....	30
Figure 6.4: (a) Model of profile C-D; (b) Cross –section of profile line C-D.....	31
Figure 6.5: (a) Model of profile E-F; (b) Cross-section of profile E-F.....	32
Figure 6.6: (a) Model of profile G-H; (b) Cross section of profile G-H .....	33

# LIST OF TABLES

---

Table 3.1: Showing structural indices and their corresponding geological structures (Geosoft 2010;Reid, et al; Thompson, 1982) ..... 16

Table 4.1: Survey specification ..... 18

## LIST OF ABBREVIATIONS

---

2D	Two Dimensions
3D	Three Dimensions
AS	Analytical signal
ASTER	Advanced Spaceborne Thermal Emission and Reflection Radiometer
BIF	Band iron formation
DEM	Digital Elevation Model
GPS	Global positioning System
IGRF	International Geomagnetic Reference Field
SWIR	Short wave infrared System
TD	Tilt derivative
TMI	Total Magnetic Intensity
UTM	Universal Transverse Mercator projection
VD	Vertical derivative
VNIR	Visible and Near Infrared
WGS	World Geodetic System
nT	Nanotestla



# 1. INTRODUCTION

## 1.1. Background

Uganda is one of the East African countries. It shares its borders with Kenya on the East, Sudan on the North, Democratic Republic of Congo on the West and Rwanda and Tanzania on the South. It lies within the African plate, which is a continental crust that contains Archean craton that date at least 2700Ma.

This research focuses on the magnetic variation of the Singo granite in Kiboga, Central Uganda. The depth, source, subsurface and surface structures of the magnetic anomaly in Singo granite will be investigated and modelled using geophysical and remote sensing datasets. Aeromagnetic data is useful in studying the subsurface structures and it is used in this research to study and model the magnetic anomaly variation of the Singo granite. Magnetic data involves measuring the variations in the earth's magnetic field which is caused by the distribution of magnetic minerals in the rocks that make up the upper part of the earth's crust. In order to model the magnetic anomaly, the geology of the surface and subsurface must be well studied. Aeromagnetic data provides information on the – surface geology of the Singo granite. The geology of Kiboga has been studied but not much study has been carried out on modelling the magnetic patterns of the Singo granite.

## 1.2. Study area

The study area is situated in Kiboga, central region of Uganda. It is about 120kms from Kampala by road. It borders the districts of Mityana and Mubende to the South, Hoima to the north, Kibaale to the west and Nakaseke to the east. The location is between latitudes 0°55'54.06"N and 0°47'7.62"N and longitude 31°28'15.58"E and 32°14'29.57"E. The Singo granite intrudes the metasedimentary rocks that have experienced low grade metamorphism. The granite is composed of plagioclase, K-feldspar, quartz, biotite, muscovite and opaque. Alluvial gold, fluorite, Wolframite and beryl are associated with Singo granite which were economically mined in the past.



Figure 1.1: The location of the study area.

### 1.3. Previous work

Previous work has been carried out on the mineralogical and chemical composition of the rocks in the Kiboga area and Singo granite by some workers that includes (Johnson & Williams, 1961; Link et al., 2010; Nagudi et al., 2003; Nyakairu & Koeberl, 2001). However, much is not known about the geophysical studies of the Singo granite. The construction of geological models based on magnetic data helps in geological interpretation of magnetic surveys. To obtain an understanding of magnetic anomalies, there should be understanding of the geological factors that control magnetic signatures which helps in geological interpretation of magnetic surveys (Clark & Emerson, 1991; Gunn & Dentith, 1997) worked on magnetic properties of rocks. (Link, et al., 2010). Other airborne geophysical mapping tools like gamma ray spectrometry only provide information about the surface whereas magnetic anomalies show information about the subsurface and therefore, magnetic surveys provide 3D geological information. The construction of geological models based on magnetic data helps in geological interpretation.

#### 1.4. Problem statement

The Singo granite is in Central Uganda. The granite intrudes metasedimentary rocks which has experienced both contact and low-grade metamorphism. According to Nagudi (2003) there is zonation in texture, mineralogy and geochemistry from the centre and comprises mainly of plagioclase, quartz, biotite, muscovite and opaque. Also the granite is associated with some minerals like alluvial gold, fluorite Wolframite etc. (Nagudi, et al., 2003). On the Singo granite at the periphery there is high magnetic anomaly while in the middle the total magnetic intensity is low. The problem is that, the source of the magnetic anomaly around the Singo granite is unknown.

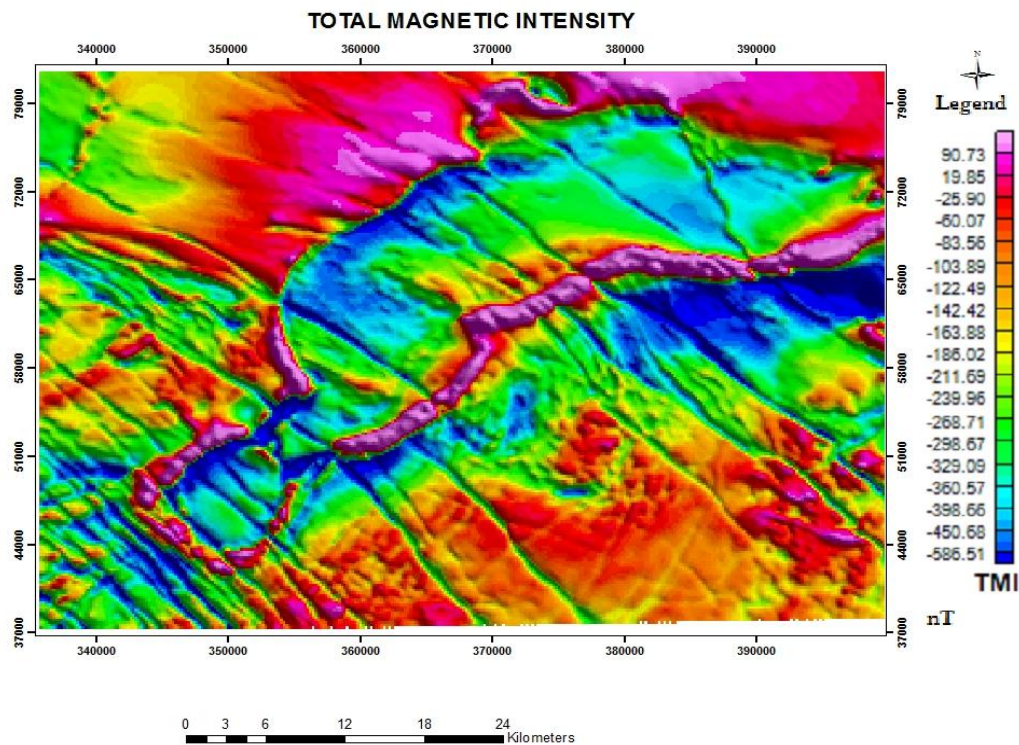


Figure 1.2: The TMI map showing the Singo granite with variation in magnetic susceptibility

Apart from the fact that Singo granite is postulated to be associated with mineralization mentioned above, it is essential for mineral exploration to obtain a complete picture of both surface and subsurface structures. This research aims to investigating the magnetic anomaly of Singo granite and its associated mineralization. It is anticipated that the granitic intrusion could act as a heat engine which is postulated by Nagudi (2003) to causing ascent of the mantle derived magma that contains mineralized fluids that were later deposited within favourable host structures and lithologies.

Integration of remote sensing and geophysical (magnetic) method has yielded result in mapping surface and subsurface geology (Lunden et al., 2001). Magnetic data can be used to delineate the source of anomaly and the geological structures in the subsurface and surface. Remote sensing data can be used to support this. The research aims to investigating the source and depth of the variation of magnetic anomaly in Singo granite and its association with mineralization in the area. Also, the relationship between the geological structures and the magnetic anomaly of Singo granite will be established.

## **1.5. Objective of the research**

### **1.5.1. General objectives**

The main objective of this research is to study the source of strong anomaly bordering the Singo granite and its possible relation to mineralization using geophysical and remote sensing data.

### **1.5.2. Specific objectives**

- ❖ To establish the magnetic susceptibility contrast between granite and its surrounding rocks.
- ❖ To determine the depth to the source of magnetic anomaly.
- ❖ To model the magnetic anomaly integrating surface and subsurface structures.
- ❖ To establish the relationship between the magnetic anomaly, the geological structures and its associated mineralization.

## **1.6. Research questions**

- Is there any compositional variation between Singo granite and its surrounding rocks?
- Does the magnetic anomaly have a shallow or a deep source?
- How can the magnetic anomaly modelling be used to determine the source of the variation of the magnetic anomaly of the Singo granite?
- What is the relationship between the magnetic anomaly, the geological structures and its associated mineralization?

## **1.7. Thesis structure**

In this research, the geological history is provided by the literature review in chapter two. The background on aeromagnetic data and the type of filtering applied is given in chapter three. In chapter four, the datasets, software and Methodology which includes a flow chart of the research is covered. The integration and interpretation of the aeromagnetic data is analyzed in chapter five. Chapter six comprises of the forward and inversion modelling of the source bodies and then the discussion of results and conclusions of this study are stated in chapter seven.

## 2. LITERATURE REVIEW

### 2.1. Regional geology

Uganda lies on the African Plate, which is one of the largest areas of continental crust covers an area of about 240,000 km<sup>2</sup>. This plate consists of accretion of small cratons welded together by mobile belts. The intense folding and metamorphism found in the mobile belts often involves the fringes of the cratons. Ages of some rocks forming some cratons have been found to be over 2.5 billion years (OMI, 2006).

Much of Uganda's geology has been studied in broad outline only and detailed work remains to be done. The geochronology is as yet incomplete. Two-thirds of the country is underlain by Precambrian rocks, comprised of Archaean, and Lower and Middle Proterozoic granites, meta-sediments and granulites (Figure 2.1). These rocks, normally classified as undifferentiated gneisses and granites, are the oldest in age and are overlain by the so-called Buganda series and Karagwe–Ankolean series. These are characterized by pelitic rocks, which have been metamorphosed to form rocks varying from slightly cleaved phyllitic mudstone and shales to mica schists.

Cenozoic rift valley sediments and tertiary and Pleistocene volcanics occur in a few areas and cover less than 10% of the country. The western part of the country is bounded by the rift valley, which is underlain by sediments made up of a mixture of sand, silts and clay. Other recent sediments are found in various places as a result of erosion to valleys and magmatic outflows from volcanic eruptions. The granitic metamorphic rocks in the Ugandan portion of the Tanzanian shield have commonly been described by the term basement

complex (Woldai, 2010). The different radiometric ages for the major Precambrian units of Uganda is shown

in the diagram. The length of the data bars includes the uncertainty in the ages. The granulite facies metamorphism of the Watian sedimentary- volcanic assemblage at close to 2900my and the intrusion of the Masaba granulite are the earliest recorded events in the Uganda basement complex. Later at about 2550m.y. a second period of regional metamorphism was widespread throughout the basement and the Aruan metamorphism is one which is known to be common throughout the continental regions and is seen as a period of granitisation and amphibolites grade metamorphism. The Buganda- Toro – Kibaran belt as suffered widespread metamorphism at about 1800m.y. while the Mirian sediments which form a northern extension of the Karagwe-Ankolean system recrystallized and formed during a tectonic metamorphism phase close to 1000m.y. The Mozambique orogeny has affected the Uganda basement complex about 650m.y. Later post Orogenic deformation is seen in the various shear zone (Leggo, 1974).

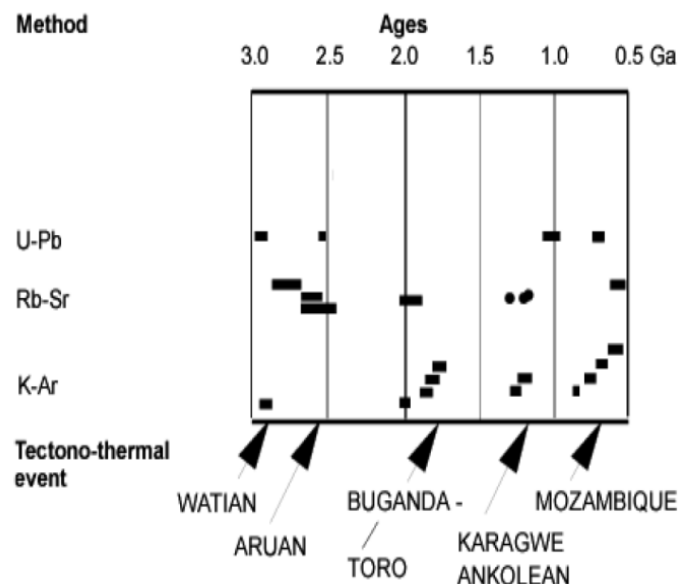


Figure 2.1: Simplified diagram showing isotopic age (bars) of Precambrian tectono-thermal veins in Uganda (Leggo, 1974).

### 2.1.1. Basement complex

The basement complex (Figure 2.2) occupies the larger areas of Uganda which consists of high grade metamorphic gneisses and amphibolites, granulites, magmatic and granitic rocks (Gabert, 1990). It constitutes the oldest tectonic unit and consists mostly of granitic gneisses usually of medium grained texture. Basement complex has been dated at 2880Ma (Leggo, 1974). According to Gabert (1990) the basement complex is unconformably overlain by the Archean Nyanzian system.

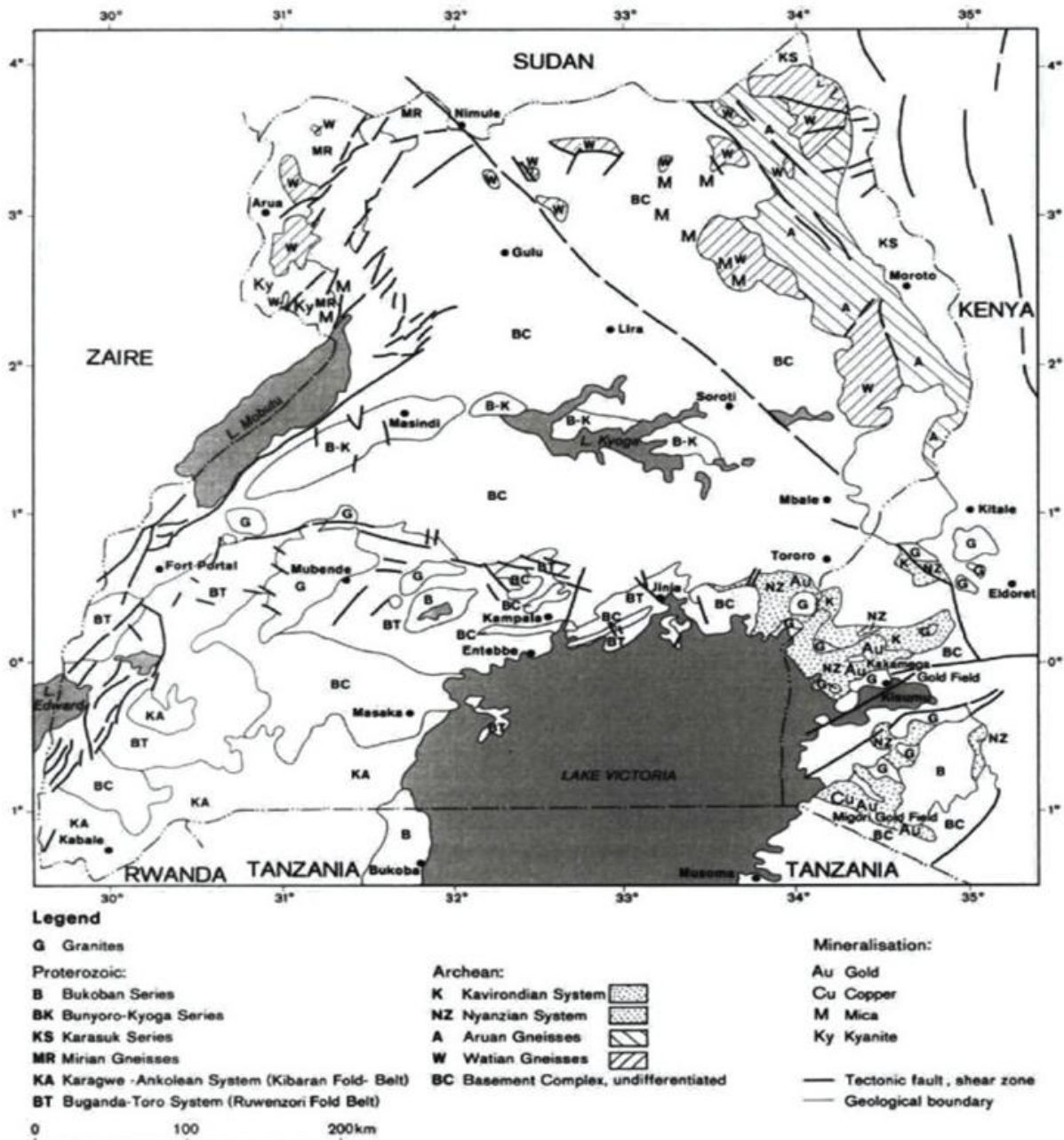


Figure 2.2: Geology of Uganda simplified after (Gabert, 1990)

### 2.1.2. Nyanzian Sequence

The Nyanzian sequence which unconformably overlain the basement complex, extends from Southeast Uganda into Southwest Kenya and is composed of a lower succession of mainly rhyolites, porphyries, tuffs and basalts and a higher succession of cherty quartzites, shales, greywacke and banded ironstones (Gabert, 1990). The metamorphic grade is very low. This system comprises the sequence of dominantly

volcanic rocks of basic composition and poorly sorted sediments that form greenstone belts occurring within the basement complex of eastern Uganda, they are subdivided into an upper and a lower series marked by the upward transition from rocks of basic to acidic composition (OMI, 2006).

The upper series of the Nyanzian sequence consists of an assemblage of flows, volcanic ash and various sediments in the form of lavas of acidic (or felsic) composition, tuff, ferruginous chert, BIF with subordinate pelite. The lower series is characterized by extensive “greenstone” flows of what was once basalt, or andesite in which pillow lava structures are sometimes displayed. It consists of sediments that form greenstone belts in the east of the country. The Nyanzian greenstones host precious metals deposits and have the potential for base metals. According to Borg (1990), both syn - and - post orogenic granitoids with several generation of felsic and intermediate dykes and sills have intruded the Nyanzian system. The schist and green stone belt of metasedimentary and metavolcanic rocks in Nyanzian exhibits low metamorphic grade which pass into migmatite, banded gneiss and other rock in the granulite facies (McConnel, 1972).

#### ❖ Mineralization

There is gold mineralization in all stratigraphic units except for the granitic rocks. The gold mineralization in Uganda is of six different types: These are BIF hosted, shear zone type, quartz vein type, Clastic sediment, hosted alluvial/eluvial and massive sulphide type deposits (Borg, et al., 1990).

- Shear gold hosted: - The E-W generally trending mineralized shear zones host significant gold mineralization are mined commercially and artisanal scale. Host rocks are mafic volcanic and locally the contact zones between chert and tuff within BIF. The host rocks around the shear zones is mineralized with pyrite and native gold which is replacing magnetic layers.
- Quartz vein type: - Gold has been mined on a small scale from several large quartz veins, which occur in various rock types e.g. volcanic rock but quartz veins in granitoids rocks are barren.
- The BIF hosted strata bound is the biggest gold producer in the past which includes the Geita mine and Jubilee reef deposits.
- Clastic sediment hosted: - The gold mineralization occurs in metasediments and in conglomerate and quartzites which were derived from the subsequent erosion of uplifted Nyanzian units.
- The massive sulphide deposit is known from limited diamond drilling and is hosted by mafic volcanic.
- Alluvial/eluvial gold occurrences are mined by local mining cooperatives and illegal miners. They are described as gold occurrence which is associated with secondary placers.

#### 2.1.3. Lower Proterozoic mobile belt

This comprises the Buganda-Toro system which extensively overlies the basement. Much of the South, west and central parts of Uganda are occupied by Buganda Toro system and it extends from Jinja to the Rwenzori Mountains in western Uganda (Nyakairu & Koeberl, 2001). According to Hopgood (1970), the Buganda –Toro system is older than 1800Ma; and includes argillite, amphibolites, and phyllites. There are dykes and pegmatite that intruded the Proterozoic including granite massifs. Also the continental rifting has caused the formation of some ore deposits.

#### 2.1.4. Middle-upper Proterozoic Mobile belt

This comprises of Karagwe-Ankolean group (K-A), a sequence of slightly metamorphosed sedimentary rocks that covers the Southwest Uganda (Buchwaldt et al., 2008). The Karagwe-Ankolean group includes argillite, quartzite, sandstones, conglomerates and calcareous rocks which rest unconformably on the Buganda-Toro system (Hopgood, 1970).

**2.1.5. Upper Proterozoic sediments**

This comprises of Singo, Mityana and Bukopban series which are found in various parts of Uganda. Singo series overlies the Buganda- Toro system in the west central Uganda, whereas the Mityana and Bukoban series occur in the central and South-west along the shores of Lake Victoria where they continue into Tanzania as Bukoban series.

**2.2. Geology of Kiboga Area**

According to Johnson & Williams (1961), Kiboga area consists of basement complex, comprising the Buganda-Toro system, Karagwe-Ankolean system and the Bukoban System.

**2.2.1. General geology of the area**

The granitic gneisses which are the oldest in the area are considered to be part of the basement complex. The granitic gneisses are cut by granites, which ages are not known. The Buganda series comprising of muscovite- biotite gneisses, quartzite, schists, phyllites, slates and fine- grained sandstone are on top of the basement complex rocks that were later folded and metamorphosed which were eroded to produce a mature surface before deposition of the Singo series, a sequence of conglomerates and sandstones with rare shale bands. The Singo and Mubende granite batholiths were then emplaced (Johnson & Williams, 1961; Nyakairu et al., 2001).

The continuous denudation (i.e. the long-term sum of processes that cause the wearing away of the earth's surface leading to a reduction elevation) exposed the granites and left the rocks of the Singo series in disconnected massifs, which now form high plateau.

The Mityana series, which consists of conglomerates, arkoses, sandstones and silicified rocks, was deposited on a very irregular surface in a series of small basins and valleys. Figure (2.3) shows the probable geological sequence of Uganda (Johnson & Williams, 1961).

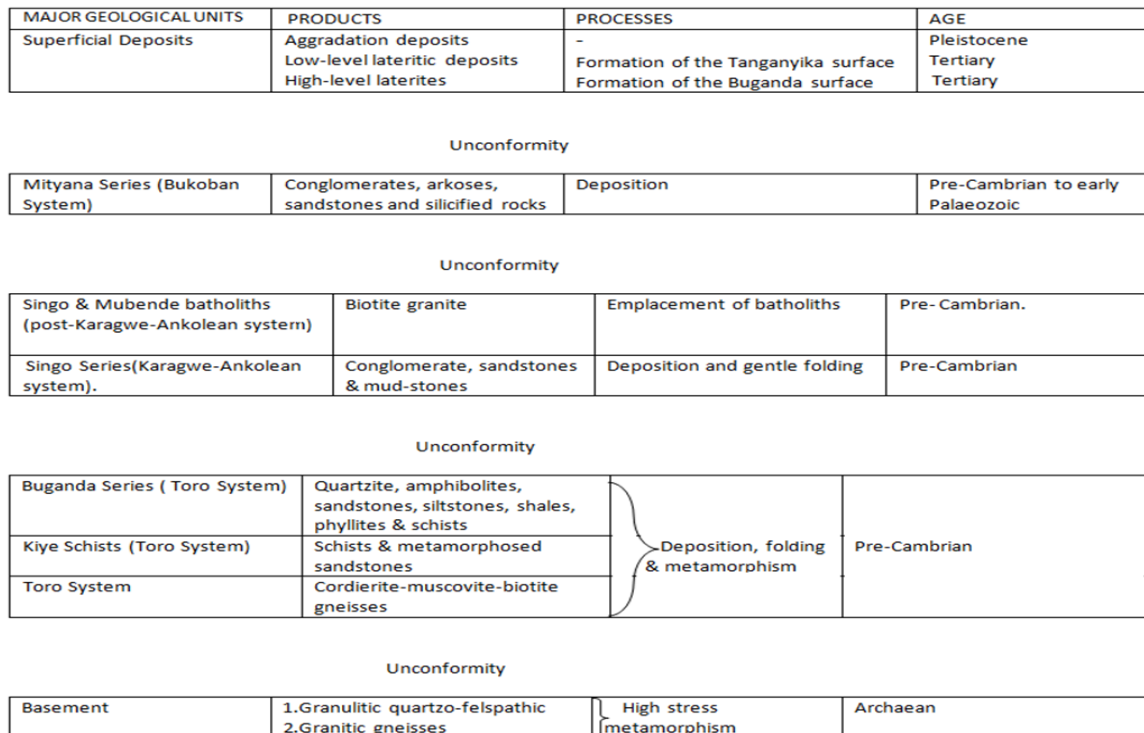


Figure 2.3: Probable geological sequence of Uganda after (Johnson & Williams, 1961)

## 2.2.2 The Granitic Gneisses (basement complex)

The granitic gneisses form large hills east of the main Kampala-Hoima road in the vicinity of Kiboga. They are poorly foliated rocks with feldspar porphyroblasts consisting of quartz, feldspar and biotite. The granitic rocks in the basement complex at Kabutemba are leucocratic granites which carry xenoliths. In this area the granite outcrops are surrounded by soils which contain fragments of a coarse tourmaline-quartz aggregate.

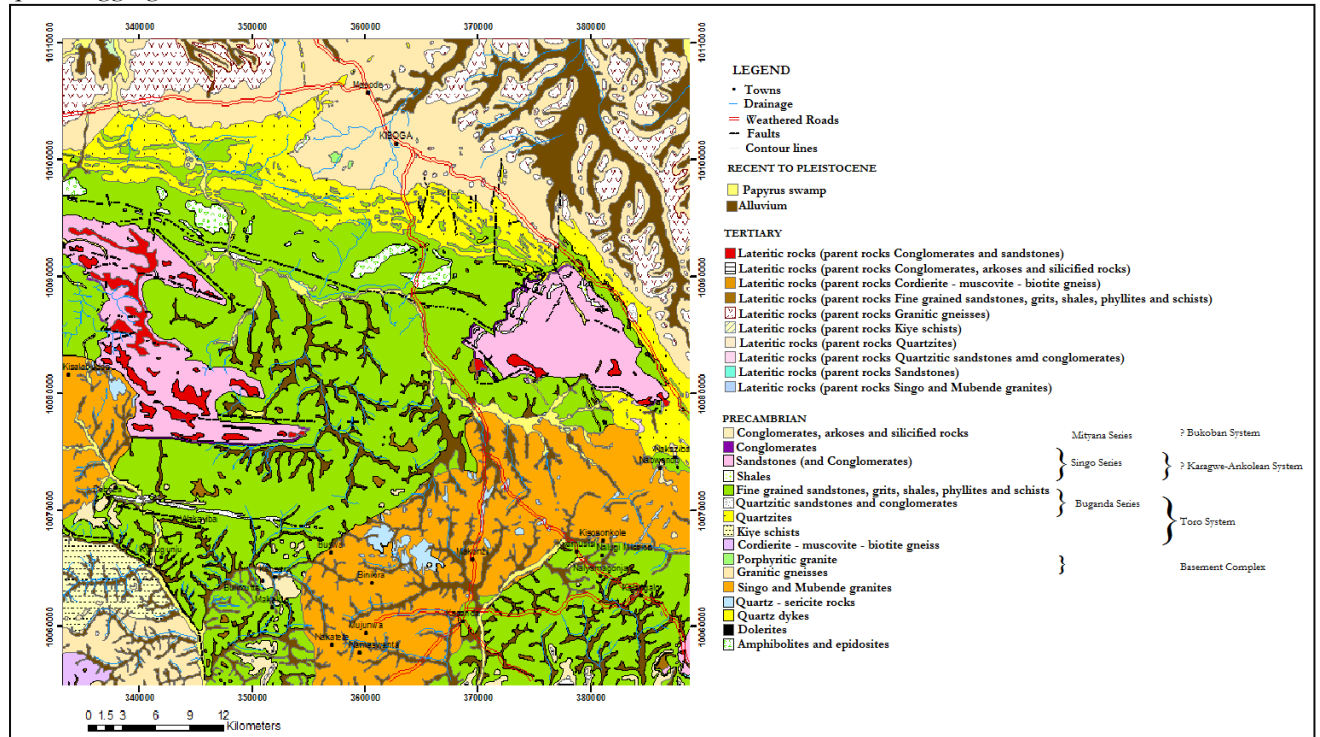


Figure 2.4: Geological map of Kiboga area after (Johnson & Williams, 1961)

- **Structures**

The few basement complex outcrops in the north consist of banded granitic gneisses with a vertical foliation which aligned at N20-35°. In vicinity of Kiboga town, much of these trends are not visible due to granitisation cover that resulted in poorly foliated rocks with porphyroblastic feldspar. The vertical planar structures found in the Kagobe-Kigando area which are parallel to the strike of the quartzite are found in the basement gneisses which indicates that locally the rocks of the Basement complex became involved in the orogeny which affected the Buganda series.

## 2.2.3 The Buganda series

Within the Buganda series, quartzite associated with amphibolites is present which is dominantly argillaceous and consist of slates and siltstones to the south. The pink and grey quartzitic sandstones which grades into white quartzite form a prominent feature that runs eastward from Mubende granite at Debeza to the boundary of the Singo granite. The regional metamorphism which occurred in the area increases southwards with the pelitic rocks metamorphosed into sericite and muscovite schists. Along the boundary of the veins in sericite and muscovite schists, abundant muscovite is present. The basal quartzite shows differences of colour, texture and structures; e.g. various shades of pink, brown, grey and light purple. Different in texture is caused by recrystallisation and deformation. There are quartz dykes occurring along fault zones at Tewenezinwa, Magi and to the north-east of Kasolo. The pelitic and semi-pelitic rocks occupies the greater part of the Buganda series. The metamorphism increases from north to south.

- **Structures**

The axes of folding in the Buganda series have two major trends in the north. In the east the dominant trend is N45°W, while to the west the alignment is east-west. Between these there is a gentle arc interrupted by a zone of chaotic folding over the basement complex.

#### **2.2.4 The Kiye Schists**

The Kiye Schists comprise of metamorphosed sandstones and semi-pelitic rocks. The structures and the metamorphic grade between the mentioned rocks on each side of the valley indicate that a fault separates the unmetamorphosed slates and siltstones of the Buganda series to the north from the metamorphosed Kiye schists to the south. At the southern boundary of the Kiye schists, the rocks consist of recrystallized quartz, cordierite altered to sericite, chlorite, biotite and oligoclase feldspar. The rock of Kiye schists has undergone three phases of metamorphism which produced cordierite, biotite and chlorite in the northern part while the rock in the southern part has undergone two stages of metamorphism: the first produced cordierite, plagioclase feldspar and biotite and the second caused the development of muscovite.

- **Structures**

The structures in the northern and southern parts of the Kiye series are different. The sandstone horizons and cleavage are present in the north. The interbedded semi-pelitic rocks are characterized by a highly developed strain-slip cleavage. The minor structures suggest that these rocks were initially thrown into tight folds with the development of cleavage. The sub-parallel of the strain cleavage which follows that both the initial folding and the refolding occurred on nearly the same axes, which suggests that they were closely related and they may represent different phases of the same orogeny. The cordierite-muscovite metamorphism followed the folding, which indicates the period of temporary quietness in deformation.

#### **2.2.5 The Singo series**

It consists of conglomerates and sandstones with some patches of shale bands which were faulted. The deposition of the Singo series followed the folding, metamorphism and erosion of the Buganda series. Quartz-hematite veins cut the conglomerates at Busanyi and there are fault breccias between the Singo series and the Buganda series.

- **Structures**

The rocks of the Singo series are folded in the Kyato-Mpologoma area. The attitude of the rocks of the Singo series has suggested that they have been gently folded. The fault zones at Tewenezinwa, Magi and north Kasolo might probably be older than the Singo series. The basal quartzites of the Buganda series up to one mile have been displayed by the sinistral tear faults. These fault zones are occupied mainly by sheared quartz, but the rocks really resemble quartz dykes.

#### **2.2.6 The Mityana series**

The rocks of the Mityana series rest unconformably on the Kiye schists, the Buganda series, the Mubende and Singo granites. The rock consists of conglomerates, arkoses and sandstones in the lower part and very fine-grained silicified rocks at the upper part. The conglomerate is composed of quartzite, quartz vein and dolerite while the arkoses consists of quartz grains, kaolin and opaque minerals.

#### **2.2.7 The Singo granite**

The Singo granite batholith in western central Uganda covers an area of about 700km<sup>2</sup> (see Figure 2.3). It belongs to the Buganda-Toro system. The parallel nature of bedding planes of the country rocks to the granite contact in some places, suggest the emplacement of the Singo granite with the country rocks happening at the same time (Nagudi, et al., 2003). The granite is cut with aplite dykes, quartz veins, hematite veins, breccias and shear zones, steep joints and sinistral faults. The major part of the batholiths is covered by dense vegetation and swamps and weathered rock outcrops. The batholithic granite is arc-shaped extending in a north-east direction from the Kaungera area to Bukunya and Kasanda and eastward to Bukomero. The batholithic granite intrudes into the Buganda series or metasediment with finely defined cross cutting contacts (Johnson & Williams, 1961). The granite is massive, coarse grained and

grayish in colour along the contact, although pink and red shades are frequent in the central part of the rock. Dykes and irregular bodies of sericitised granite are widely spread. In some places foliation is present which is defined by parallel alignment of long axes of some of the feldspar phenocrysts. The margins of this granite are characterized by a rapid increase in both the number and size of microcline phenocrysts as they grade into the coarse-grained granite. There are joints in rock which are randomly oriented.

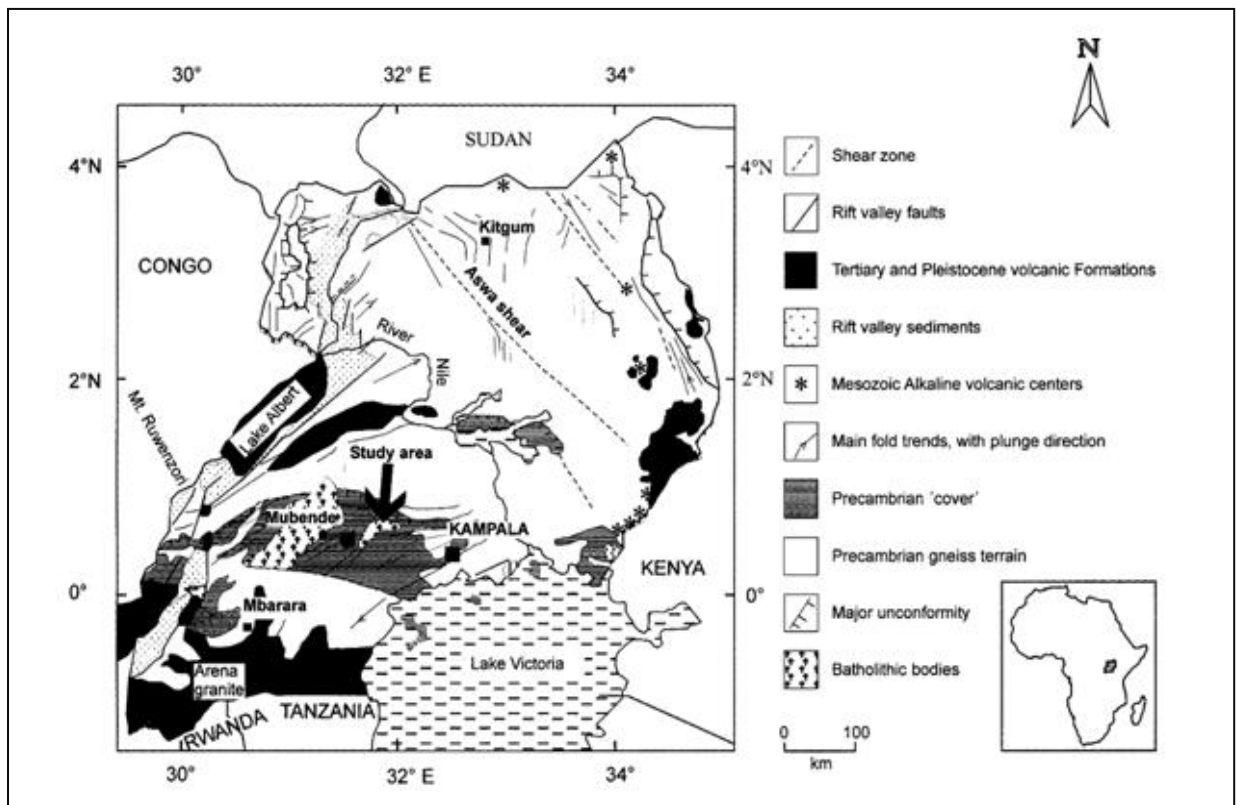


Figure 2.5: Simplified geological map of Uganda showing the location of Singo granite and some structural features (modified after MacDonald (1966).

- **Intrusion**

The Singo batholiths is characterized by quartz and sericite which normally form linear features but some may have a rounded outcrop as on Lusungwe Hill, or are V- shaped as at Biwalwe. Dykes of similar strike form typical ridges between Kasanda and Bukunya and some dykes in this area also trend south-east. At further east the dominant strike is north-east, parallel to the major jointing in that area. In the study area there are no actual contacts between the dykes and the surrounding granite has been seen, but they appear to be sharp and their position can often be deduced to within a yard or two. In some localities the feldspars of the enclosing granite may be sericitised up to 100 yards from the contacts (Williams, 2009). According to (Johnson & Williams, 1961), all field and petrographic evidence shows that the quartz-sericite rocks represent zones of alteration in the granite. Their dyke-like and lenticular shapes and their intrusion into the country rocks, suggest that they represent granite which were emplaced after main batholith was in position and began to consolidate. The aplite dykes in the area are composed of fine-grained aggregates of quartz, microcline and albite-oligoclase, with scattered flakes of muscovite. In the study area, there are present of small amount of small irregular dykes and zones of pegmatite with random orientation and along the joints in the granite, the thin quartz veins are usually not more than 2 inches thick (Johnson & Williams, 1961).

One large body identified as Xenoliths is found in the granite to the north of Naludi mission. It has been affected by granite and has been silicified and tourmalinised near its boundaries. Porphyroblastic muscovite has formed in the polytropic rocks, and the body is cut by a few thin dykes of fine-grained muscovite granite. In the marginal granite near Bukuya and in the vicinity of Bunyonddwa, there are present of Xenoliths, which are normally of Bunyonddwa, there are present of Xenoliths which are normally angular and have no preferred orientation and their contacts with the granite are usually sharp.

- **Metamorphism**

The country rocks have experienced both low grade regional and contact metamorphism (Nagudi, et al., 2003). According to Johnson & Williams (1961), the intrusion of the Singo granite had very little metamorphic effect on the country rocks. The sandstones have been chemically altered by the replacement of a quartz-muscovite-sericite aggregate and quartz-muscovite-feldspar dykes are found cutting the wall rocks. At the contact of the batholiths, breccias set in fine-grained vein are present. During the emplacement of Singo granite, there has been very little metamorphic effect on the country rocks. During this process, some indurations and silification have taken place, and enrichment of tourmaline and occasionally occurrence of haematite. The discrete flakes and porphyroblastic aggregates of muscovite are found in less metamorphosed rocks of the Buganda series. There are little indications that the fine sandstones have been metasomatically replaced in an irregular manner by a quartz-muscovite-sericite aggregate, and quartz-muscovite-feldspar dykes which are sometimes seen cutting the wall rocks. Sandy hornfels are present at the contact of the granite that were transformed into breccias set in fine-grained vein quartz. This indicates that during the emplacement of the Singo granite, the sandy hornfels become silicified.

### **2.2.8 The Mubende Batholiths**

The Mubende and Singo granite are similar and assumed to be the same age. The Mubende granite cuts across the Buganda series. The dolerite dykes in the area cut all the rocks with the exception of the Mityana Series. The Buganda series is intruded by the dolerites which are often weathered to a soft, purple rock, in which kaolinised feldspar can be recognized. In the basement granites at Kiboga and in the fault zones near Kasega, Magi and Kiganda, there is present of weathered dykes.

## 3. Magnetic petrophysics

### 3.1. Airborne magnetic survey

Geophysics is the science of studying the earth's physical properties. In other words, is the science which deals with investigating the Earth, using the methods and techniques of physics. It contributes to an understanding of the internal structure and evolution of the earth.

Geophysics in mineral exploration is based on the idea that the rock being sought has physical properties that are substantially different from the properties of the country rock. When certain physical property of a rock such as density, magnetic susceptibility, seismic velocity etc reacts differently from the surrounding rock, then it indicates an anomaly. The observed contrast between ore body and country rock depends foremost on mineralogical composition, size and depth of the ore body which also give the quantities analysis of the anomalous body.

There are many geophysical methods but magnetic method was applied in this research to determining the depth and to model the magnetic anomaly in Singo granite in order to determine the depth and source of the anomalous body. Aeromagnetic has the ability to uniformly map a geological structure in a very large area, this has made it highly suited for geological mapping (Jaques et al., 1997).

### 3.2. Rock magnetism

Rock magnetism is the study of magnetic properties of rocks, sediments and soils. Magnetisation is defined as the magnetic moment per unit volume of material and is measured in (A/m). One of the factors that determine the patterns of magnetic anomaly is the earth's crust. Rock magnetization is the total magnetism of a rock and is defined as the vector sum of the induced and remanent magnetisations (Clark, 1997).

- **Induced magnetization**

This is the component of magnetisation produced in response to an applied field i.e. induced magnetisation is created in the presence of an external magnetic field (earth's total magnetic field. All crustal rocks find themselves within the geomagnetic field and they are likely to display induced magnetisation.

- **Remanent magnetisations**

After the removal of an externally applied field the rocks and minerals may retain magnetization and thereby becoming permanent magnets. This property is known as remanent magnetisation and is manifested in different form, depending on the magnetic properties of the rocks, minerals and their geologic origin and history.

### 3.3. Influence of metamorphism

Most minerals on earth naturally magnetise some pieces of magnetite which is one of the minerals that occur in all rock types. The proportion of its occurrence in igneous, metamorphic and sedimentary rock varies and one of the factors that influence its occurrence in rocks is metamorphism. During metamorphism magnetic minerals may be created or destroyed. The parameters of magnetic susceptibility and remanent magnetization of rocks can be altered by metamorphism. According to Nagudi (2003) and Johnson (1961) contact metamorphism has occurred between the Singo granite and the country rock.

### 3.4. Magnetic susceptibility

This is a measure of the magnetic response of a material to an external magnetic field or is the degree of magnetization (both induced and remanent) of a material in response to an applied magnetic field. The susceptibility (K), measured in dimensionless units is defined as the ratio of the material magnetization (J) (per unit volume) to the external magnetic field (H):

$$J=KH..... (i)$$

Magnetic susceptibility of a material can either be positive (paramagnetic) or negative (diamagnetic) (Hunt et al., 1995). The magnetic susceptibility of a material depends on the content of paramagnetic and ferromagnetic minerals.

According to Clark (1997) magnetic susceptibility of grains can be reduced through demagnetization which depends only on weakly susceptibility of the grain materials. The susceptibility of rocks depends on accessory minerals in the rock i.e. the magnetite content in most rocks is shown in the susceptibility of the rock. Different rock types show different magnetic susceptibility (Figure 3.1). The metamorphic rock which makes up the largest part of the Earth has a wide range of magnetic susceptibilities; also, igneous rocks show wide range of magnetic properties but dykes and sills of a mafic composition do have a strong, remanent magnetisation due to rapid cooling. On aeromagnetic maps they show the clearest anomalies which cut discordantly across all rocks in the terrain. Sedimentary rocks are usually non-magnetic which sometimes show indication of buried magnetic sources below the sedimentary sequence.

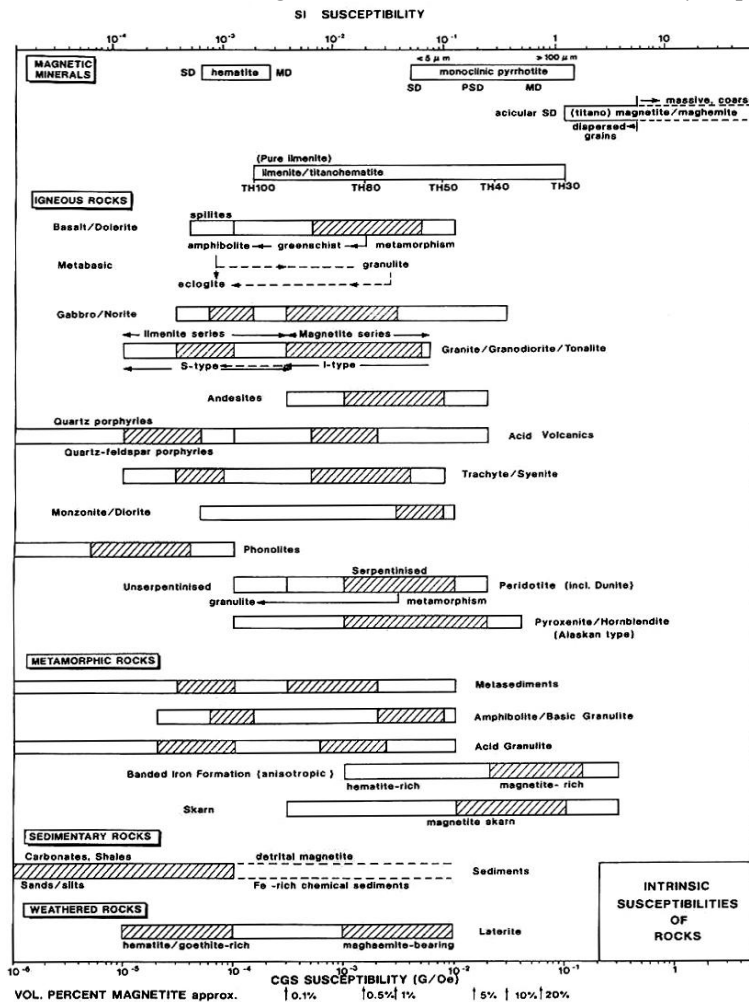


Figure 3.1: Susceptibility ranges of common rock types (from Clark & Emerson 1991)

### 3.5. Filtering of aeromagnetic data

In order to interpret the airborne magnetic data and to facilitate the interpretation, it is very useful to filter the data. The type of filtering used is described below:

- **Vertical derivatives:** These are used as an aid to the interpretation process because they enhance the detail and sharpen geophysical anomalies. It narrows the width of anomalies and so, locates the source bodies. They also enhance shallow sources, while suppressing deeper ones and gives a better resolution of closely-spaced sources.
- **Analytical signal (AS):** It is used to locating the edges of magnetic source bodies and also it defines source positions regardless of any remanence in the sources. It defines source position regardless of any remanence in the source bodies. The AS is the square root of the sum of squares of the derivatives in the x, y and z directions:

$$AS = \sqrt{dx^2 + dy^2 + dz^2} \text{ ----- (ii)}$$

- **Tilt derivative (TDR):** The combination of the tilt derivative and its total horizontal derivative are very useful for mapping shallow basement structure and mineral exploration targets (Verduzco et al., 2004). According to the latter tilt derivative (TDR) of the total magnetic intensity is defined as:

$$TDR = \tan^{-1}[VDR/THDR] \text{ ----- (iii)}$$

Where, VDR and THDR are the first vertical and horizontal derivatives respectively of the total magnetic intensity I.

$$THDR = \sqrt{(dT/dx)^2 + (dT/dy)^2} \text{ ----- (iv)}$$

The total horizontal derivative of the tilt derivative is defined as:

$$HD\_TDR = \sqrt{(dTDR/dx)^2 + (dTDR/dy)^2} \text{ ----- (v)}$$

### 3.6. Field inversion

3D Euler deconvolution process is mainly to produce a map that shows the locations and depths of the geologic sources of magnetic or a gravity anomaly observed. This method was used to estimate the depth and also as an indication of the causative bodies from the airborne magnetic field (Geosoft., 2010). The method uses gradients, either measured or calculated. To calculate the 3D Euler deconvolution the data does not need to be pole-reduced (Reid et al., 1990) and the technique can outline confined sources, vertical pipes, dykes and contacts.

The 3D Euler deconvolution uses x, y, and z derivatives grids to obtain its results. It is illustrated in Figure (3.2).

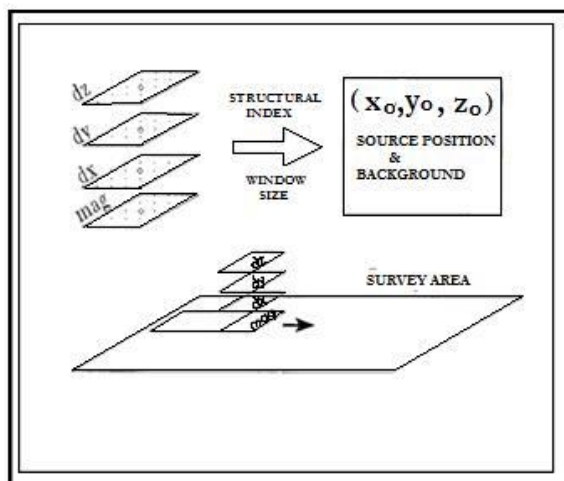


Figure 3.2: Schematic method of Euler deconvolution. Input data; dx, dy and dz are x,y and z derivative grids respectively of the input and mag = magnetic field input grid (from Kuttikul 1995).

There are two types of techniques for calculating Euler deconvolution and they are *standard* and *located* Euler technique provided by Oasis Montaj. It obtains its solution by inverting Euler’s homogeneity equation over a window of data over every grid point. The standard Euler method produces more solutions than the located method. The located Euler deconvolution technique calculates the analytical signal, find or locate peaks in analytical signal grid and uses these locations for Euler deconvolution. This method produces fewer solutions than the Euler method.

The following parameters are important when using 3D Euler deconvolution method:

1. Structural index (SI)
2. Window size and position
3. Grid cell size

**Structural index:** Structural index is a measure of the rate of change of the field with distance (Thompson, 1982). This is an algorithm parameter which the user must select in applying the technique. The structural index is also a measure of how sharp an anomaly is relative to its depth and many geologic features have distinctive fall-off rates or structural indices. The value of the SI parameter depends on the type of source body one is looking for and the type of potential field data used.

Structural Index	Magnetic model	Geological model
0.0	Contact	contact
0.5	Thick step	Fault
1.0	Sill/dyke	Sill/dyke
2.0	Pipe	Pipe/cylinder
3.0	Sphere	Sphere

Table 3.1: Showing structural indices and their corresponding geological structures (Geosoft 2010; Reid, et al; Thompson, 1982)

**Window size and position:** Another important algorithm parameters for 3D Euler deconvolution method is window size and position. It was concluded by (Kuttikul, 1995) that anomalies arising from deeper sources are poorly represented in small window, this makes small window undesirable (Barbosa et al., 1999) and (Reid, et al., 1990).

**Grid cell size:** Grid cell size is another important algorithm to select when using 3D Euler deconvolution method. A grid cell size is the smallest element in a 2D map and all features on a map can be related to this basic unit.

## 4. DATA SETS AND METHODOLOGY

This chapter covers the data sets, softwares and the methodology used in this research. All the data sets used in this research were sets to the same projection (WGS 84, zone 36N).

### 4.1. Description of data sets

#### 4.1.1. Geological map and mineral occurrence point

The geological map is of scale 1: 100,000 and covers the entire area of Kiboga. The map was compiled, drawn and published by Geological survey Department of Uganda in 1960 and is based upon the work of Uganda.

#### 4.1.2. Remote sensing data

Remote sensing is a tool for image interpretation. This process involves analysis, processing and interpretation of geo-spatial data sets in order to extract geological information (Thurmond et al., 2006).

The remote sensed datasets used in this study include:

- **SRTM DEM**

A digital elevation model (DEM) is a digital map of the elevation of an area on the earth. It can also be defined as a representation of earth's surface topography (Teichrieb & Kelner, 2007). DEM is very useful for lineament extraction (Abarca, 2006) because it shows the surface of the earth's geomorphology. From DEM data, geological lineaments like faults has been extracted in Kenya (Gloaguen et al., 2007). In this study, the hill shaded DEM will be overlaid with ASTER image to extract the structural features. The data was acquired in 2008.

- **ASTER**

The Advanced Space-borne Thermal Emission and reflection Radiometer (ASTER) sensor is a multi-Spectral imaging system. The ASTER data consist of 14 bands in the electromagnetic spectrum with 6 bands in the short wave infrared (SWIR) with 30m spatial resolution, 5 bands in the in the thermal infrared (TIR) with 90m spatial resolution and 3 bands in the visible and near infrared (VNIR) with 15m spatial resolution. It has better and enhanced spatial resolution especially in the visible and near infrared, also, wide spectral coverage than LANDSAT. The VNIR measures visible reflected radiation in three spectral bands between 0.52 and 0.86, the SWIR measures reflected radiation in six spectral bands between 1.6 and 2.43 and thermal infrared (TIR) between 8.125 and 11.65m. The data was acquired in 2008.

The ASTER acquired from the study area was mosaicked using ENVI and ERDAS software. This is important in order to facilitate further image enhancement approaches. The mosaic image was geo-referenced to WGS 84, Zone 36N. The layers were stacked together and subset to cover the study area. Aster image colour composites, band 7, 3, 1 were applied for lineament delineation.

#### 4.1.3. Geophysical data

The airborne gamma-ray spectrometry and aeromagnetic data were acquired during the same survey in Uganda by FUGRO airborne survey from 7<sup>th</sup> December, 2006 to 31<sup>st</sup> May, 2007. The radiometric and geometric corrections have been made. Table 4.1 show the survey specification for the aeromagnetic data.

<b>Magnetic Data Recording interval</b>	0.1 seconds
<b>Radiometric Data Recording interval</b>	1 second
<b>Sensors mean Terrain clearance</b>	80 metres
<b>Flight line spacing</b>	200 metres
<b>Tie line spacing</b>	2000 metres
<b>Flight line Trend</b>	035 degrees
<b>Tie line Trend</b>	125 degrees

Table 4.1: Survey specification

## 4.2. Software used

### ❖ OASIS

OASIS Montaj from Geosoft was used to process the airborne geophysical data i.e. both the airborne magnetic and gamma ray data. The theory and processes used by OASIS for calculations written in the magnetic background are also available on the website and manual (Geosoft, 2010).

### ❖ Arc Map

ESRI Arcmap 10.0 was used for processing and interpreting of the available geological data. To hill shade DEM. Also, for good visualizations and capture various maps in a database.

### ❖ Potent

Potent is software for modelling the magnetic and gravitational effects of subsurface structures i.e. cross sectional modelling. Potent v4.09 is from geophysical software solutions, Australia. The software program is designed to compare and match the observed and calculated field. The theory for modelling is available on (Potent, 2010).

### ❖ Erdas software

Erdas software is used for visualization, analysis and processing of images. In this research it was used to mosaic and process ASTER.

## 4.3. Methodology

In order to achieve the aims and objectives, as well as to answer the research questions, the following steps were carried out. This research was carried out in three stages, which are: pre-field work, field work and post field work. The methodology is illustrated by a flow chart in Figure 4.1.

### 4.3.1. Pre-field work

This phase involves literature review to study the geology of the area and all datasets used in this study was brought to the same projection during the course of the research. The aeromagnetic data (Total magnetic intensity map) was prepared for guide on the field. Also, planning of the field work was also done.

### 4.3.2. Field work

The main purpose of field work is for ground truthing. The field work was carried out by walking transects perpendicular to anomaly across the Singo granite, collecting the magnetic susceptibility of the variation in the anomaly using susceptibility meter. The magnetic susceptibility of the different lithologies with their geographic location was collected. Fifty-five (55) geographic locations were recorded and at

least two (2) magnetic susceptibility values for each location were obtained and rock samples were picked from different area. The kappa meter was the instrument used for collecting the magnetic susceptibility. The magnetic susceptibility values are displayed on the total magnetic intensity map (appendix 02). The field data with their geographic locations are shown in appendix 03.

#### 4.3.3. Post-field work

After the field work, the tasks carried out include analyzing of the field data, 3D Euler deconvolution, modelling of the source of anomaly, processing of other datasets which includes mosaicking of the ASTER data. Afterwards, Principal component analysis (PCA) and band combinations were chosen for structural interpretations. The DEM was hill shaded and was combined with the ASTER to extract surface lineaments. The subsurface information was extracted from the aeromagnetic data. All results were finally interpreted.

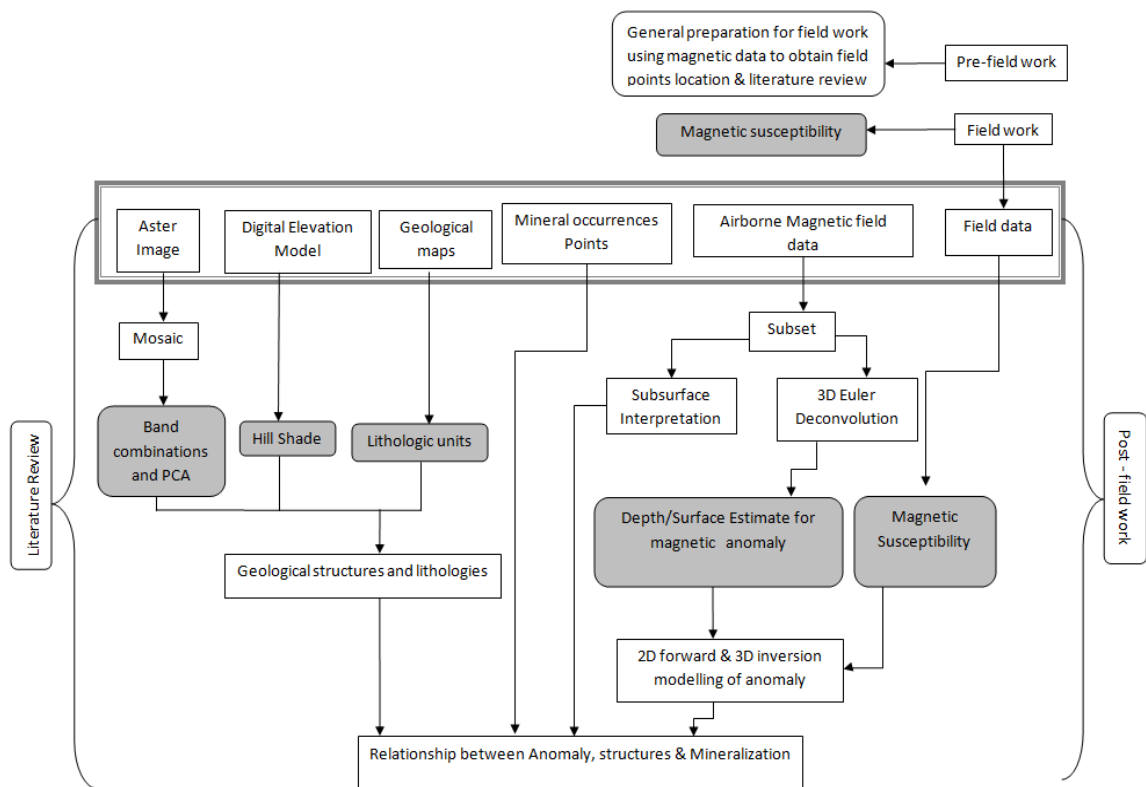


Figure 4.1: Flow chart showing the research methodology

## 4.4. 3D Euler deconvolution

### 4.4.1. Depth results

The inversion technique 3D Euler deconvolution was applied to the total magnetic intensity field to locate the depth of the anomaly. The total magnetic intensity data was gridded using 200 m spacing with minimum curvature algorithm available in the geosoft software package. The selected grid spacing is appropriate for selecting a window size which is 15, indicating the grid cell area used to compute the Euler solutions. The grid cell size determines the window size. The processing steps carried out in this research are shown in the flow chart seen in Figure (4.2).

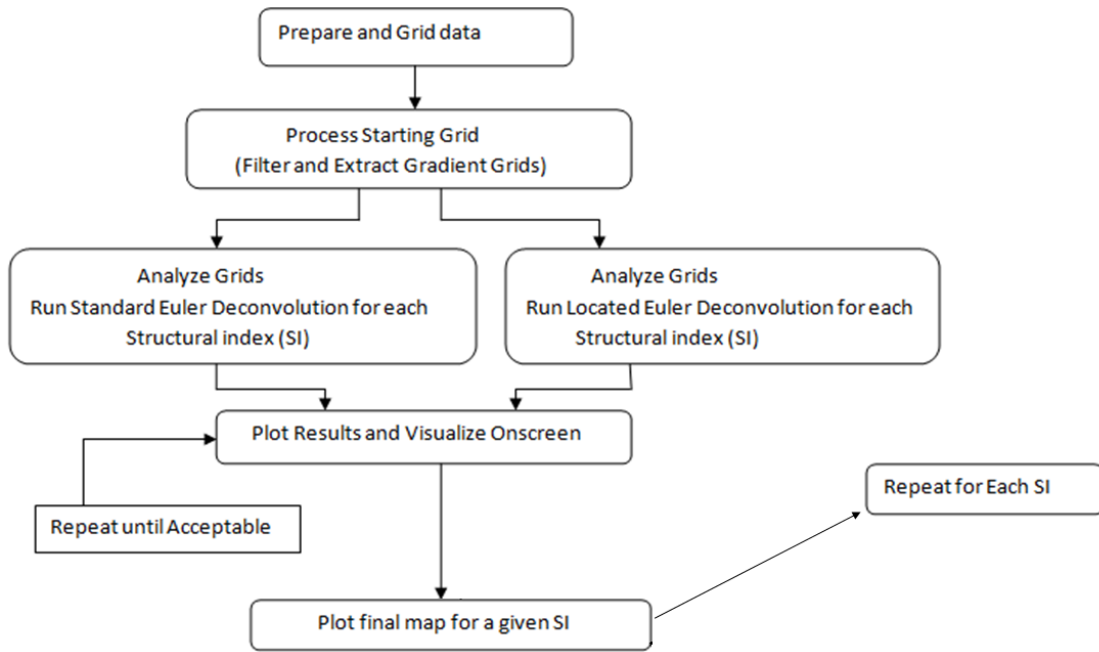


Figure 4.2: Steps followed for 3D Euler deconvolution

## 5. Interpretation & integration

In this chapter, the results of the field work and geological interpretation of the study area was carried out. The interpretation was based on information obtained from the magnetic data and other remote sensing data coupled with knowledge from geology of the area (based on literature review).

### 5.1. Field work

Magnetic susceptibility values obtained from part of the study area visited were on different five lithologies which are granites, metasediments, quartzites, quartz sericite, and Sandstone. The Magnetic susceptibility values range from 0.00 to 21.70. Several measurements were taken at different point and average of the values was calculated for each point. Geological map of the study area which show cross-section (A-B) of some of the lithologies as well as the field location points where the magnetic susceptibility were obtained is in Figure (5.1a). The field location points are also display on magnetic map in appendix 01.

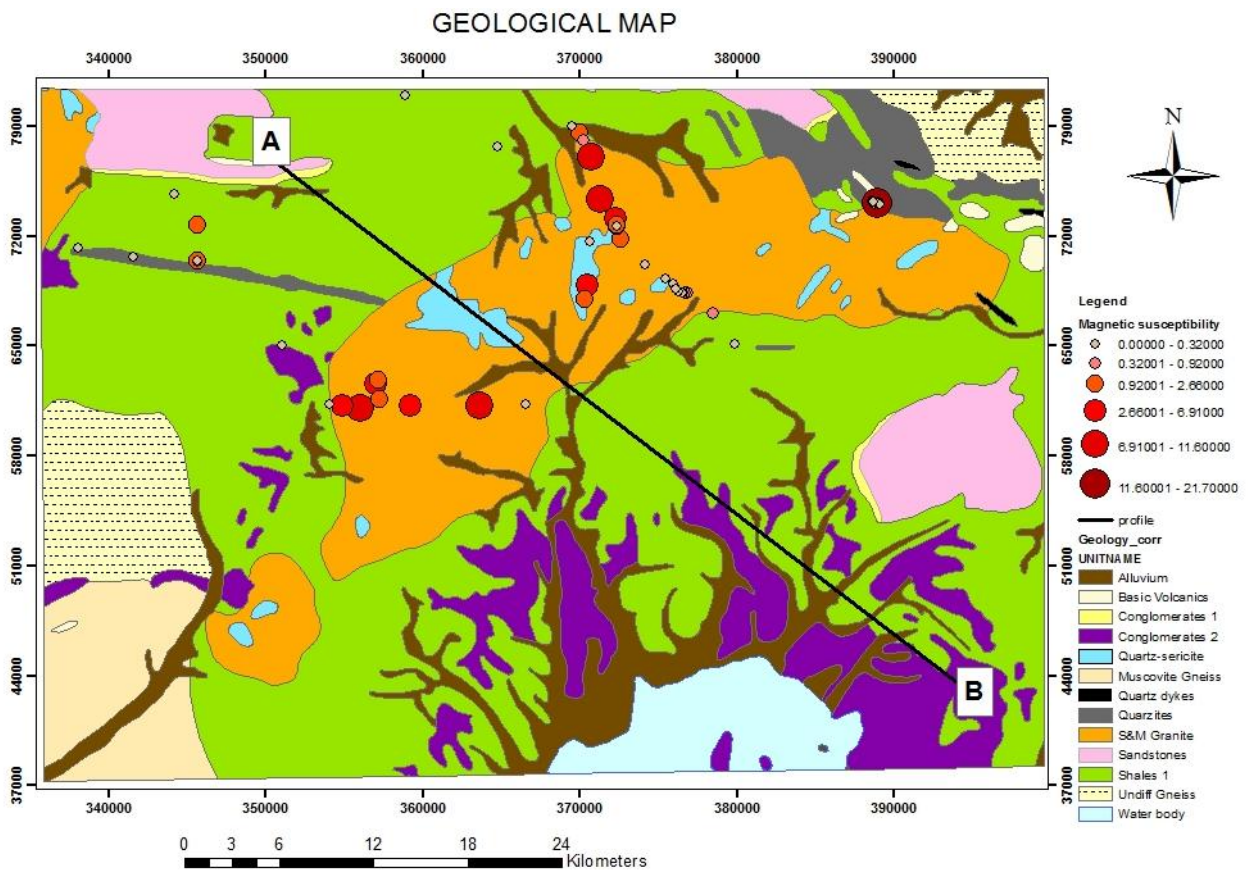


Figure 5.1a: Cross section A-B and visited points displayed on geological map

The cross-section A-B was made to cover the different lithologies in the area. The profile (A-B) extends from the eastern part of the study area to the western part and crosses almost all the lithologies in the area. There are five lithologies in the area. The lithologies are shown in geological cross section and stratigraphical column in Figure (5.1b and 5.1c) respectively.

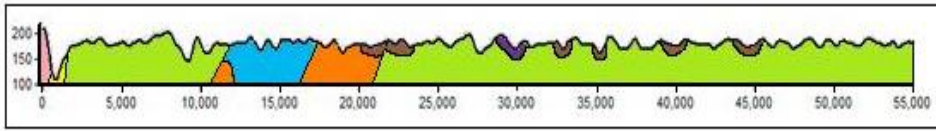


Figure 5.1b: Geological cross section of profile A-B, 5.1c stratigraphy column for profile A-B

STRATIGRAPHY COLUMN		
	AGE	ROCK TYPES
	Recent to pleistocene	Alluvium
	Tertiary	Quartzitic Sandstone & conglomerate
Bahoban System	Nilyra Series	Conglomerates, arkoses, silicified rock
Kagege Anoban	Singo Series	Conglomerates & sandstone
Tono System	Buganda series	Fine grained sandstones, grits, shales, phyllites and Schists (metasediments)
		Singo granite
		Quartz Sericite rock

The Magnetic susceptibility values were plotted to show their variation on different lithologies. Box plot was used to display this variation; however sandstone and quartz-sericite lithologies have only two reading and thus could not be displayed as box plot. The box plot result is shown in Figure (5.2a). The result shows that granite has the highest magnetic susceptibility compared to other lithologies. The two lithologies (sandstone and quartz-sericite) have the smallest magnetic susceptibility. They are displayed as histogram with other lithologies in Figure (5.2b). The cross-section A-B was made to cover the different lithologies in the area. The profile (A-B) extends from the eastern part of the study area to the western part and crosses almost all the lithologies in the area

**Box Plot**

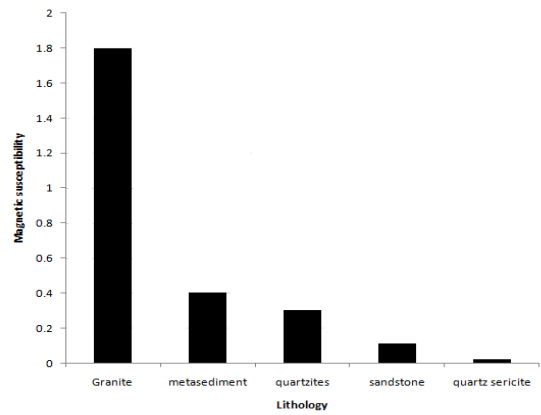
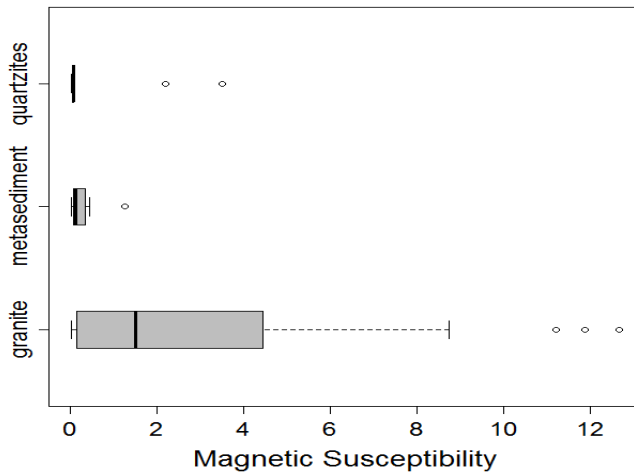
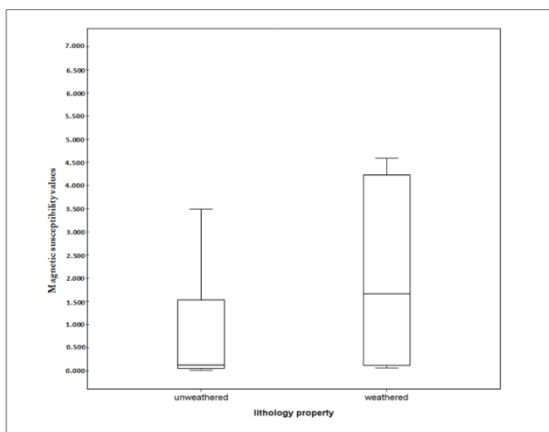


Figure 5.2: (a) Box plot showing the different values of magnetic susceptibilities of the three lithologies; (b) Histogram showing variation in the five lithologies.



The high Magnetic susceptibility values obtained in the granite lithology were grouped into weathered and unweathered rock. Variation occurs in the magnetic susceptibility values within the two groups shown as box plot in Figure (5.3). Interpretation on this is discussed in later chapter and detailed magnetic susceptibility values are found in Appendix 03.

Figure 5.3: Magnetic susceptibilities values for weathered and unweathered granite

## 5.2. Aeromagnetic Data

### 5.2.1. Total magnetic intensity

The total magnetic intensity map shown in Figure (5.4) is characterized by relatively low and moderate magnetic field with two laterally extensive mainly magnetic anomalies to the NW and SE of the study area. The amplitudes of this moderate magnetic field range from -103 to -142 nT. Linear traces of high frequency magnetic sources follow the entire outer margin of Singo granite. This high frequency sources have amplitude above 90nT. On the geological map, these sources represent areas covered by metasediment which according to the mineral composition have low magnetic susceptibility.

Another high frequency but negative magnetic anomaly attains amplitudes of -585nT. This anomaly forms broad features but of variable width that seems to be associated with Singo granite, a relationship that is not distinctively defined. Other characteristics features look like dyke intrusions. These dykes that cut the broad magnetic anomalies show low magnetic intensity which might be due to weathered zone around them.

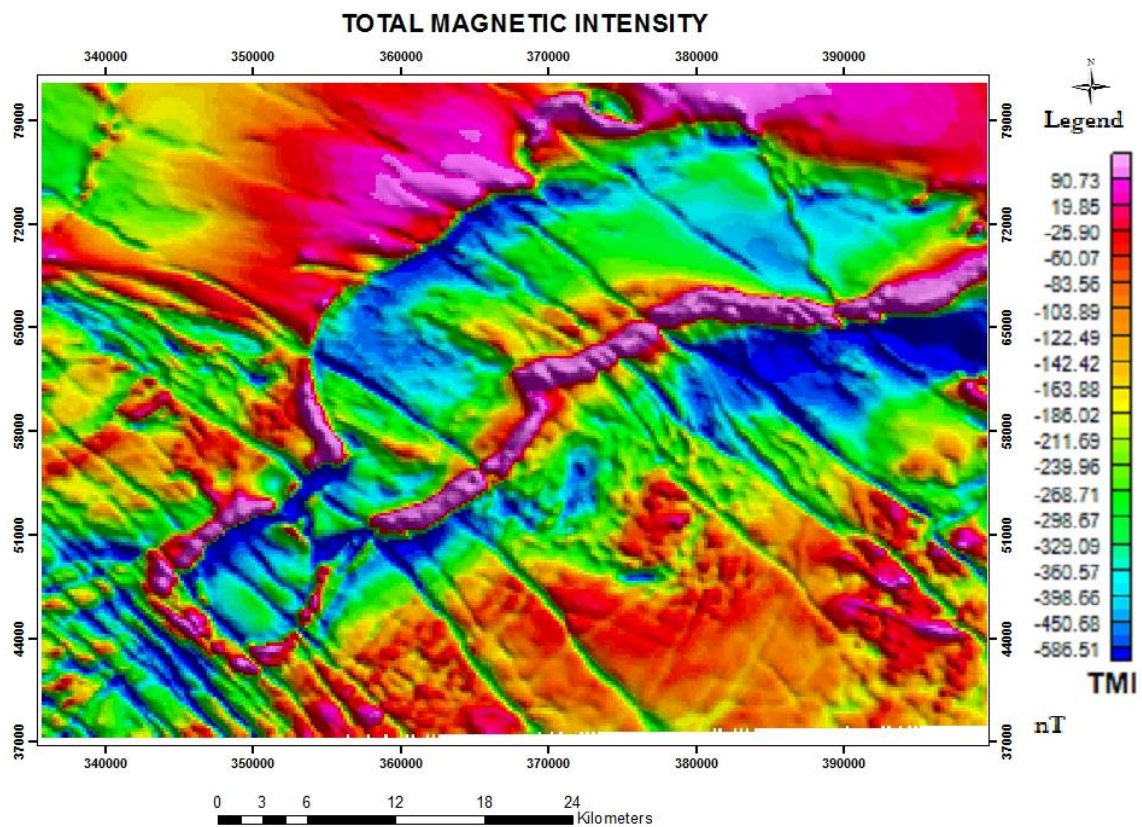


Figure 5.4: Diagram of Total magnetic intensity

### 5.2.2. Analytical signal

The analytical signal map obtained over the study area is shown in Figure (5.5). The analytical signal shows more information about the magnetic susceptibility of the area. Some area characterized by low magnetic intensity in TMI show as high in Analytical signal map (e.g. dykes and metasediment towards south-west of the study area). Notably, the analytical signal has filtered out the near surface sources possibly related to weathering of metasediments. The high frequency sources around Singo granite are clearly defined by continuous sources that break in part to form isolated sources. This offers additional support that these sources could be linked to xenoliths with tourmalised margin.

The dykes intrusion interpreted to have low magnetic susceptibility in Figure 5.4 are clearly defined by high frequency sources, this indicates that they are covered by weathered materials as inferred earlier. The strong magnetic susceptibility of these dykes indicates that they represent dolerite dykes.

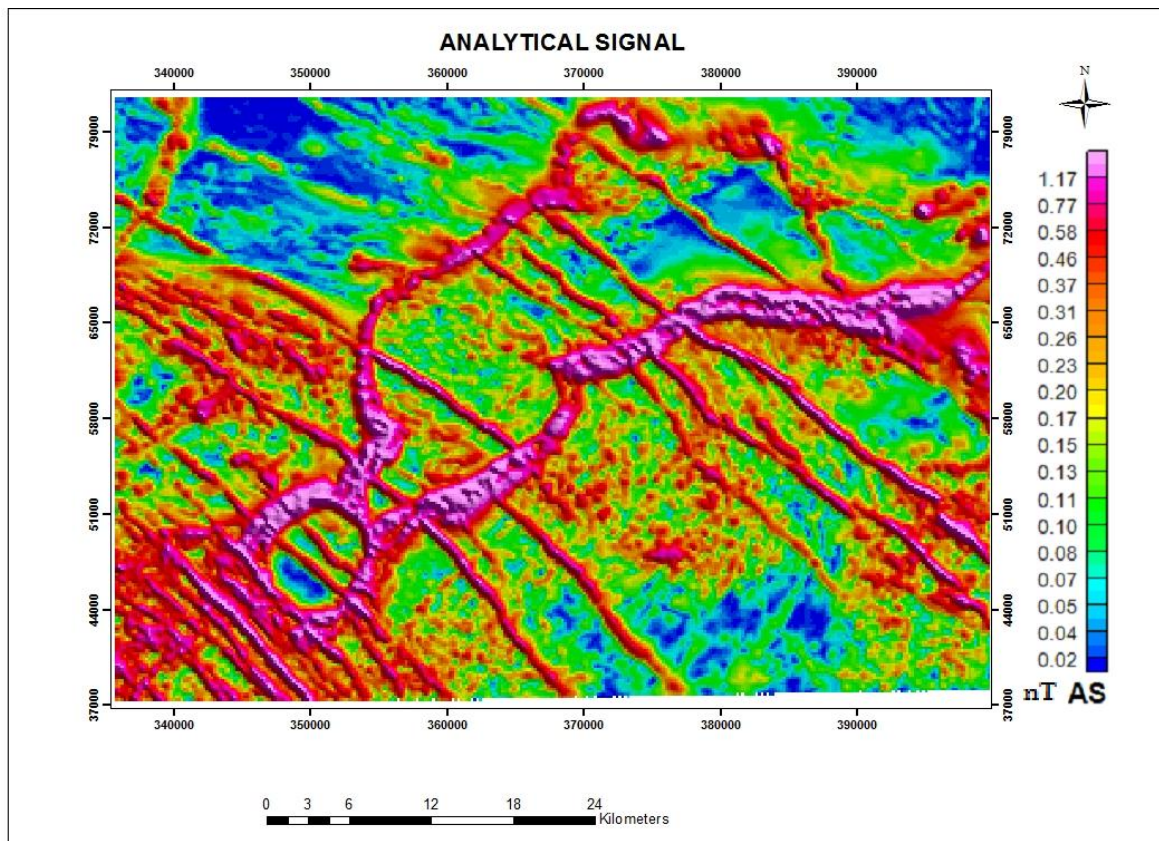


Figure 5.5: Resulting map from analytical signal

### 5.2.3. Tilt Derivative

The tilt derivative map clearly shows the outline of the Singo granite as the major feature, which also shows the prominent dykes oriented in the NE and SW direction and the NW-SE direction (Figure 5.6). However, the EW oriented features are not depicted on the tilt derivative map. A very unique characteristics' feature of tilt derivative map with the shearing of the north west south east structures to form curve linear structure near southern margin of Singo granite, a marginal deflection of NW-SE structures is also observed near the southern margin of Singo granite where shearing is intensified. These shearing effects have not been identified earlier and could be possibly being related to magmatic intrusion of the granite or a regional tectonic event. In deed the shearing has dislocated the southern margin of Singo granite. Indicating it's a younger episode compared to intrusion of granite. It is noted that the shearing was localized on a small area on the southern margin of the granite (shown in yellow circle A and B).

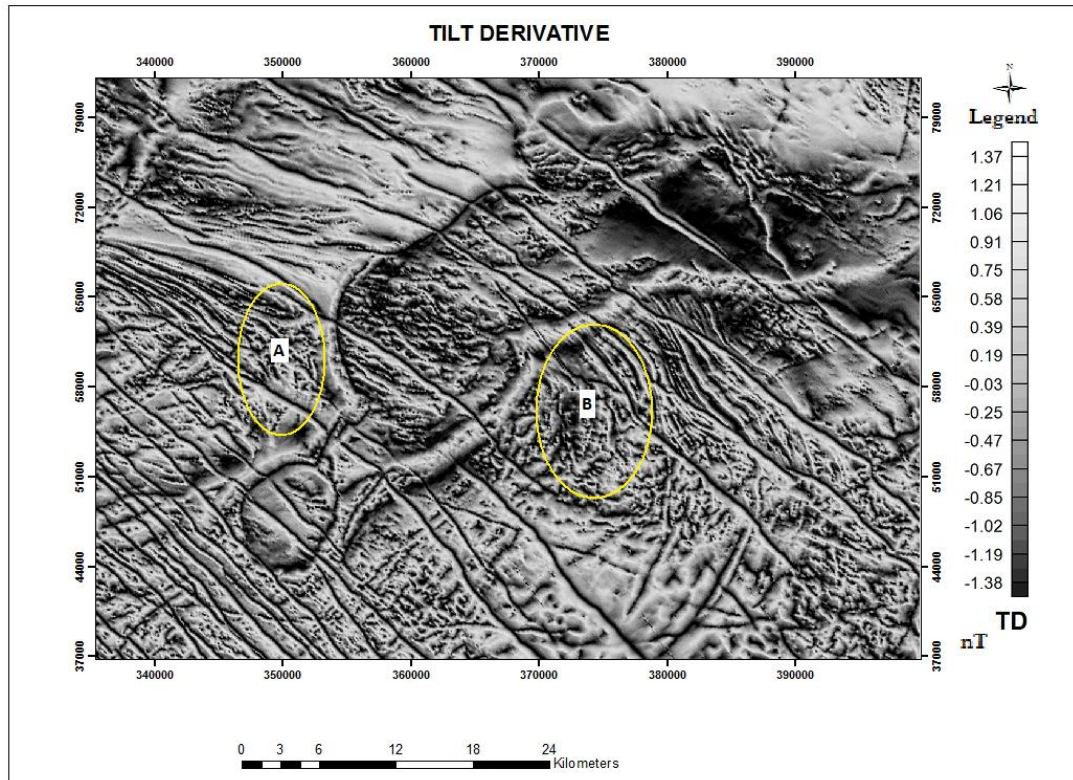


Figure 5.6: Diagram of tilt derivative

#### 5.2.4. Horizontal derivative of tilt

The horizontal derivative of tilt derivative map shown in Figure (5.7) is useful for mapping shallow basement structures similar to the other magnetic maps, which show that the outline of Singo granite is slightly subdued. The strong NW-SE oriented dykes or structures that are deflected further westwards after crossing the northern margin of the Singo granite. These NE-SW dykes cut across all the other geological structures indicating that they are the youngest in age. The westward deflection could possibly be related to shearing because of the deformation by compressive stress. An increased number of SE-SW structures are observed in Figure (5.7) as compared to other maps. These structures are clearly cut across by the NW-SE structures indicating that they are older. There is no identifiable contact between outline of Singo granite and the NE-SW structures to determine the age's relationship.

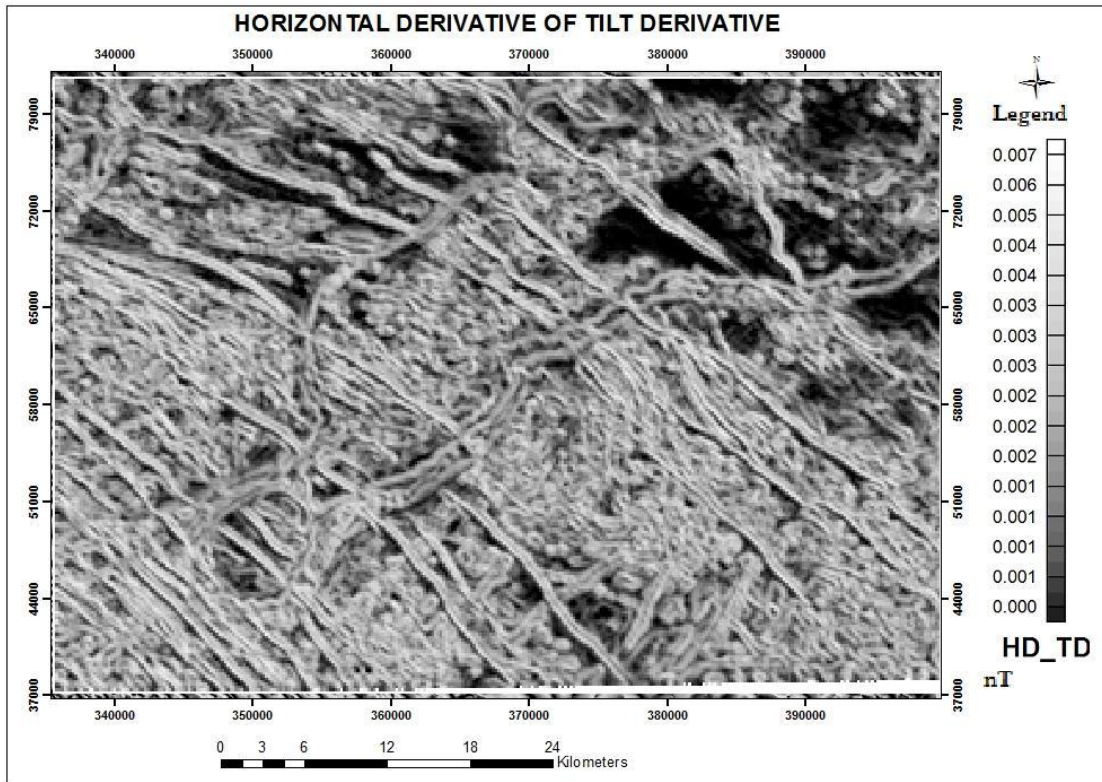


Figure 5.7: Diagram of Horizontal derivative of tilt

### 5.2.5. Vertical derivative

The vertical derivative map (Figure 5.8) shows similar structure as described under Total Magnetic Intensity map in Figure (5.6). Further to this, the central part of the study area has two sub circular features somehow related to the shearing effect. A similar feature is observed on the south-eastern end, but is poorly defined.

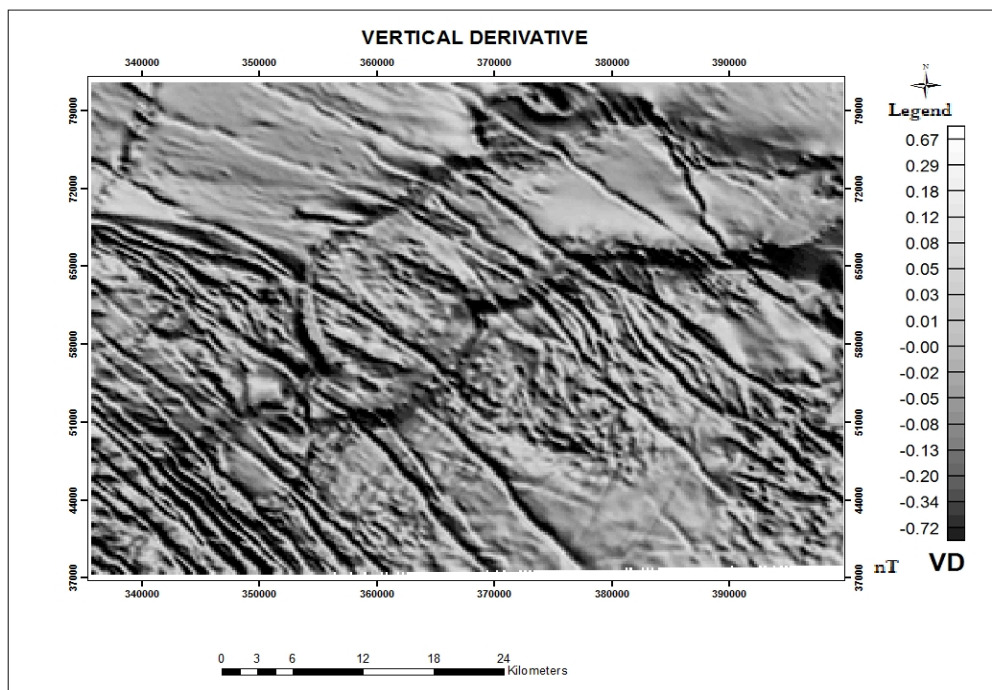


Figure 5.8: Diagram of Vertical derivative

### 5.2.6. 3D Euler deconvolution (Depth result)

According to Reid (1990), the Euler deconvolution Structural Index (SI) for dykes =1. The depths of the anomaly in Singo granite and its periphery were determined using the Euler deconvolution method. The dykes and the periphery of Singo granite which have shallow source are associated with focused solutions (15 by 200 (grid cells 3000meters)) window size. Depth obtained with structural index 1, flying height 80m, and maximum distance to accept 1500 which is more accurate. The depth result of the anomaly is illustrated in Figure (5.9). Generally, the depth result of the anomaly in the area is 550meters which is relatively deep.

The results from the 3D Euler Deconvolution shows two distinct features in the area namely: linear features and isolated aggregate with deep sources. The linear features can further be grouped into two: the NW-SE and the NE-SW structures. The NW-SE structures are the most widespread in the study area. Although they trend NW-SE in the southern area, incline further westwards. The magnetic source of these structures is confined largely within a zone of 300-400m (as indicated by the deep blue colour). However, a few of these sources occur at depth of shallow depth of 100-200m. A section of the north-western corner has a unique range from 200-300m which is indeed not widespread.

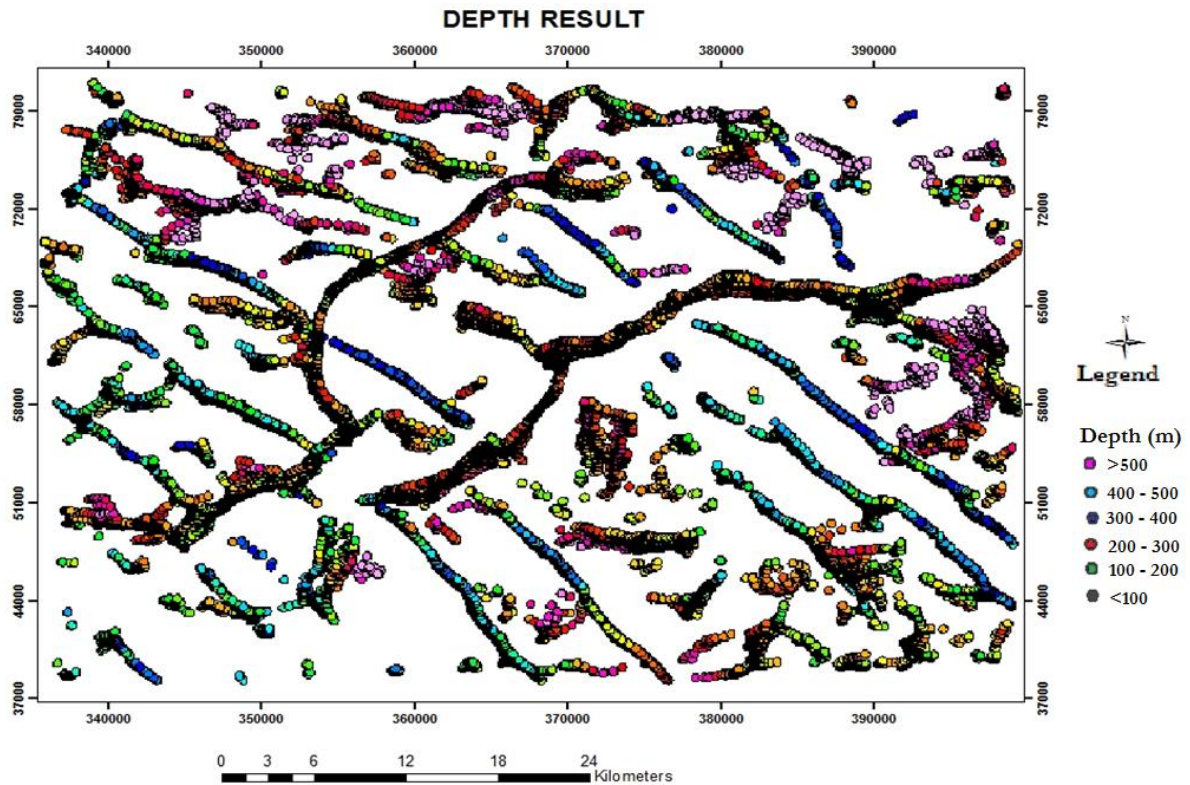


Figure 5.9: The Depth result from 3D Euler Deconvolution

NE-SW trending linear features characterize the central part of the study area. The main linear features occur as two sub-parallel lineaments trending NE-SW, which cover about two thirds of the area. In its south western end, it become circular and then breaks again to form to form a complete circle at its termination point. The magnetic sources along this NE-SW are mostly shallow (100-200m). The circular feature on the south western end has few sources to a depth of 200-300m. Another important characteristic is that the sub-parallel NE-SE structures are cut by the NW-SE structures, indicating a strong persistence of the NW-SE dykes. Geologically, the NE-SW marks the Singo granite which is cut by the NW-SE dykes, indicative that the granite intrusion is much older than the dyke.

The isolated deep sources occurred mainly on the northern part of the study area running in a poorly defined E-W trend. Another significant cluster is found on the eastern part of the study area. On the western side only significant and much localized sources are found there. The main characteristic of these sources is that they attain depth greater than 500m.

### 5.3. Integration of Dataset

The most occurring geological formation of the study area is metasediment which contain phyllites, schists, sandstones, Quartzites, amphibolites, sandstones, shale. The rocks are spread out across the entire area except where they are intruded by other geological formations or covered by alluvium deposits (see Figure 5.1). The Singo granite covers about a quarter of the study area cutting across the metasediments in a generally NW-SE direction. The boundary between the batholiths and the country rock is sharply defined. The Singo granite has minor intrusions largely composed of quartz sericite (altered rock). These intrusions dominantly occur at the centre and north edge of the granite.

Integration of the data sets shows that SRTM DEM and ASTER data express surface structures while the magnetic data showed the subsurface structures (Figure 5.10a and 5.10b). The minerals present in the study area (gold, tin and tungsten) and are confined largely within the drainage system and also fall on some of the dykes in the study area but there is no enough evidence to show the relationship between the structures and mineral occurrence points (Figure 5.10b).

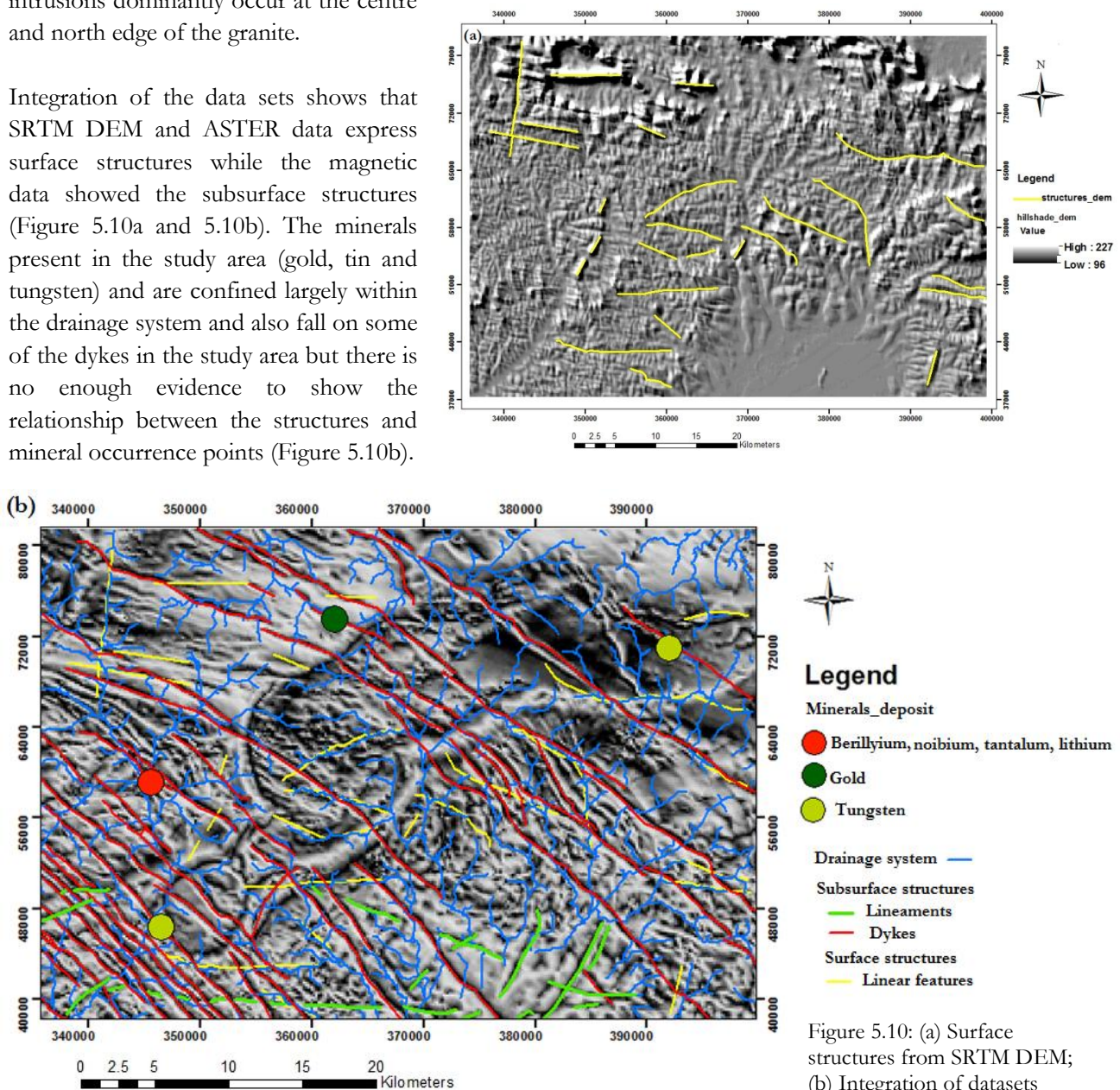


Figure 5.10: (a) Surface structures from SRTM DEM; (b) Integration of datasets

## 6. Modelling of aeromagnetic anomaly

### 6.1. Forward and inversion modelling

Forward and inversion modelling are the two different ways to model the geology in the region, based on the aeromagnetic data. The forward modelling is useful in estimating the distribution of the aeromagnetic anomaly source for any type of body and this is done when the model parameters are adjusted manually in order to improve the fit between the observed field and the calculated field, while inversion modelling takes place when the computer program adjust the modelled magnetic body shape or the model parameters (which are position and physical properties of the model) automatically to make or improve the fit between the calculated field and the observed field. In potent, the inversion scheme is very easy to modify. This process can be done on any combination of parameters from any of the bodies. Potent is a program for modelling the magnetic and gravitational effects of subsurface structures. In this research, the potent was used to model the magnetic anomaly at the periphery of the Singo granite.

Forward modelling was applied along two constructed profiles to model the geological structures of Kiboga and Singo granite. The forward modelling was done by entering the shape of one or more geological bodies to Potent, in order to calculate their magnetic effect at the subsurface of the earth. After this, the calculated and the observed magnetic field were compared together as to get best fit between the observed and the calculated. The shapes of the bodies were adjusted and Potent recalculates the model until the calculated anomaly curve fits the observed field curve. Most times forward and inversion modelling are combined processes for modelling. Firstly, the forward modelling to calculate the model, but afterwards the inversion modelling using the first model, to refine the created model but in this research, the inversion modelling was applied after the forward modelling but there was no significant changes.

### 6.2. Methodology

Since the direction of the profile is not the same with the aeromagnetic flight line, it was not possible to import the observed values as location (x, y) and z files in Potent. In this case the analytical signal was imported into the potent, which was first uncompressed. The analytical signal (As) Geosoft v2 files format, shown in figure using Geosoft as shown in Figure (6.1a) was imported for modelling and is displayed in colour map as shown in Figure (6.1b).

Each grid point is presented as (X, Y, Z, F) observation points in potent program, with X, Y representing the horizontal coordinates; Z represents the height of the observations in meter, and F represents the AS. The profile window consists of two panes; the original observed field values in profile form are shown in the top pane, drawn as blue crosses while the red line is the calculated field (these are shown in the model figures below). The horizontal axis is the observed analytical signal (AS) values in nanotesla. The bottom pane is the cross-section pane. The vertical axis, Z, is height and so the negative values represent depth. The cross-section of the sub-surface is shown in the window, which represents the model. The green crosses represent the observation points. The cross section pane uses the same horizontal axis as the profile pane.

A subset is a sample of observations from a particular dataset. It consists of all the observations that lie within a rectangular or polygonal window. To construct the model for the magnetic data along the profiles

the depth result obtained from the standard Euler deconvolution for magnetic data was used to estimate the depth. The observed magnetic field does not fit well with the calculated field when the bodies were added initially, in this case the physical properties of the bodies representing the cause of anomaly was iterated in order to have good fit between the observed and the calculated field.

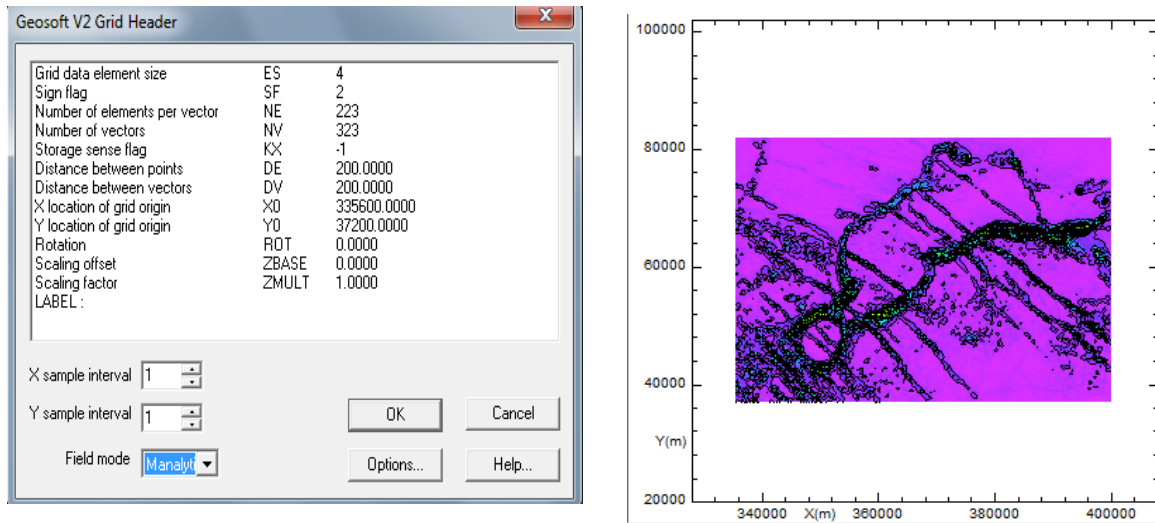


Figure 6.1: (a) Geosoft V2 Grid Header file showing the analytical signal used for the modelling; (b) Analytical signal, the horizontal axis is the distance in metre, while the vertical axis is the observed analytical signal in nanotesla

### 6.3. Conceptual geological model

In order to model the magnetic anomaly of the Singo granite, a conceptual geological model that was correlated with the magnetic anomaly at the periphery of the Singo granite was thought of before starting the modelling. To achieve this, the geological cross-section along profile line C-D, E-F and I-J in Figure (6.2) were constructed to aid the modelling. The stratigraphy column for profile lines (C-D, E-F and I-J) is the same as in Figure (5.1c).

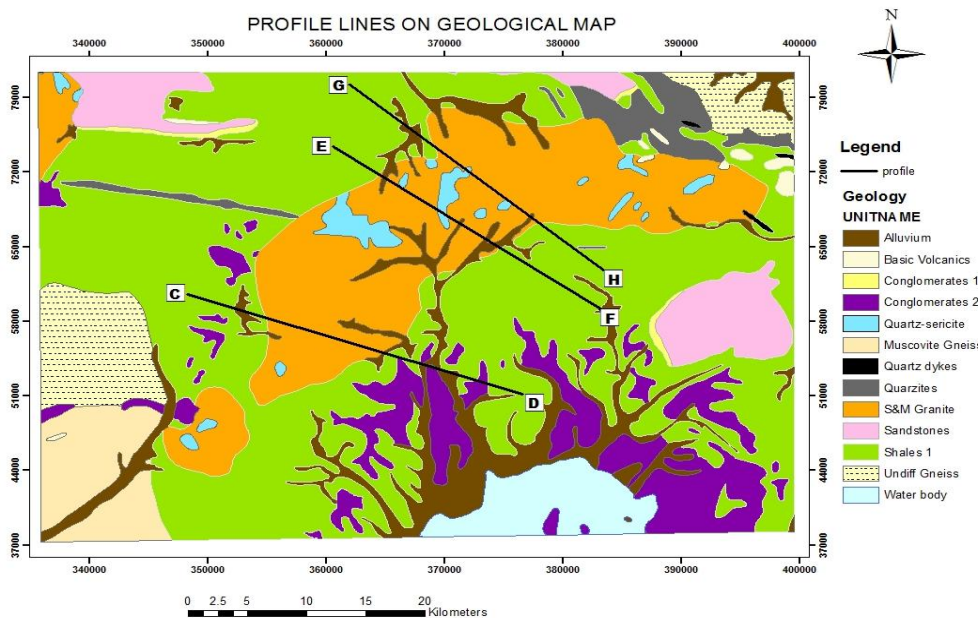


Figure 6.2: Figure showing the profile lines used for the modelling

- **Geological model of profile C-D**

The conceptual geological model was constructed based on the geological cross section. The modelling of the rocks and also the source of the magnetic anomaly with its physical properties were determined. During the qualitative interpretation of the aeromagnetic anomaly in the Singo granite, it was identified that in the geological profile C-D (Figure 6.4a and 6.4b), the magnetic anomaly was due to two different sources which are xenoliths and a dyke.

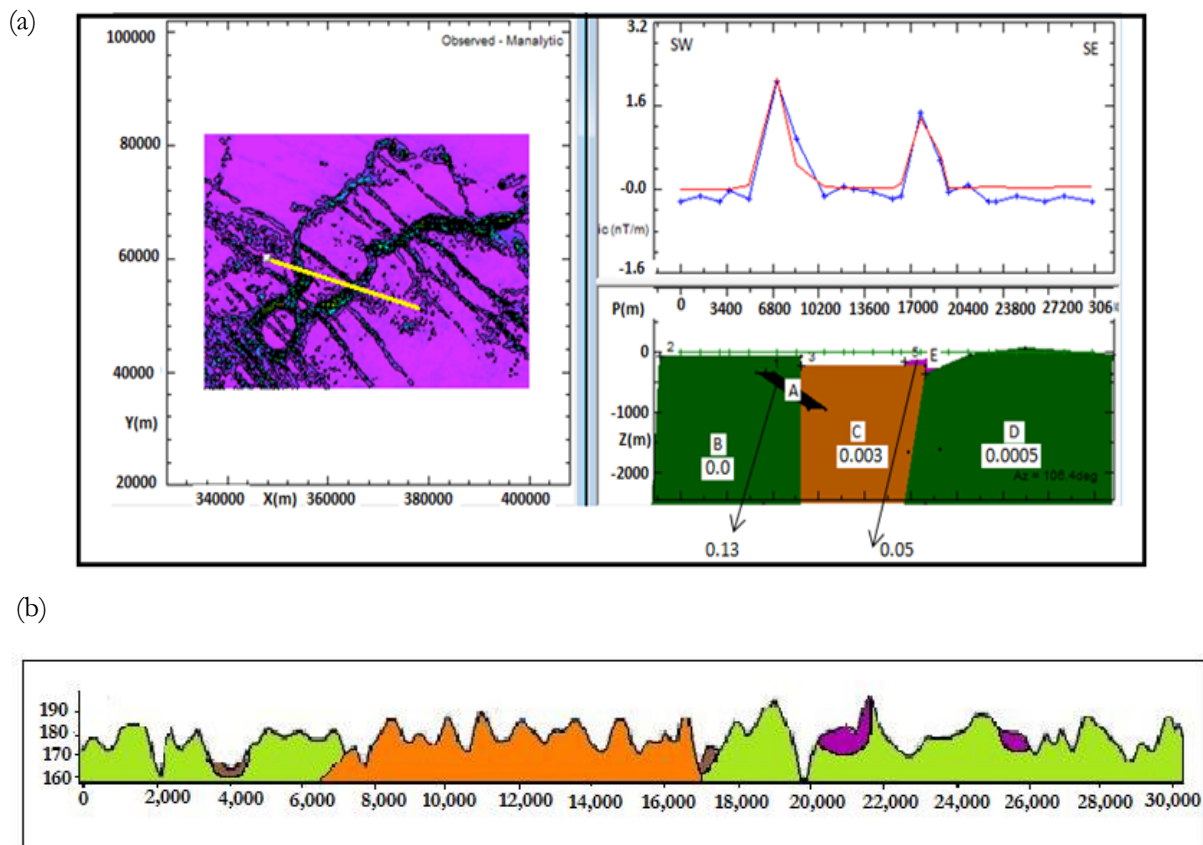


Figure 6.4: (a) Model of profile C-D; (b) Cross –section of profile line C-D

Generally, the Singo granite is an intrusion into the metasediment, the dyke tends to cut across the granite while the Xenolith is at the eastern periphery of the Singo granite. To create the geological model, the bodies were selected and made active because the Potent program (software) made the bodies inactive by default set of parameters (shape, position, physical properties). After, activating the bodies, the strength, declination and inclination of the area was set to that of Uganda.

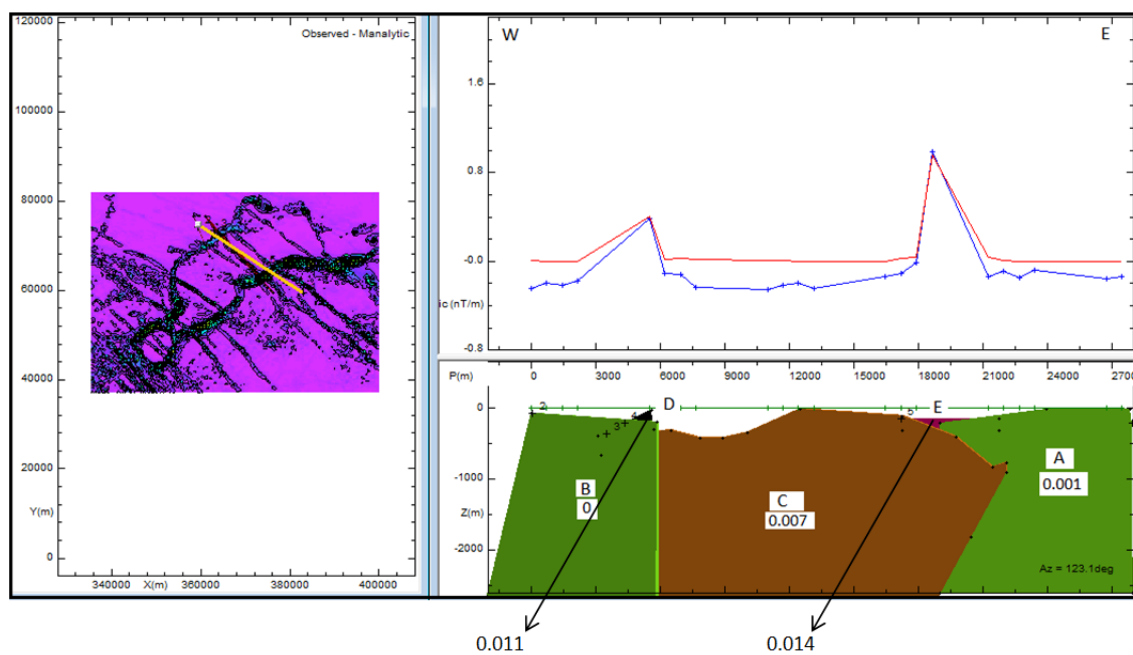
In the modelling shown above, the body A shape is a linear feature or a dyke which has a depth of 300meters which correspond with the result got from Euler deconvolution with magnetic susceptibility of 0.013. The body B and D have body shape of slab representing the metasediment while body C represent

the Singo granite. Body B has magnetic susceptibility of 0, body C has magnetic susceptibility of 0.003 and body D also is a slab with magnetic susceptibility of 0.0005. The body E which represents one of the sources of the magnetic anomaly is also a slab with depth of -167.9 with magnetic susceptibility of 0.05.

- **Geological model of profile E-F**

In this model (Figure 6.5a and 6.5b), the body A and B has a slab shape representing the metasediments with magnetic susceptibility of 0.001 and 0 respectively. Body C represents the Singo granite with slab body shape and magnetic susceptibility of 0.007. Body D and E represent the anomalous bodies. D has dyke body shape with magnetic susceptibility of 0.011 with a depth of -204meters which correspond with the result from Euler deconvolution. Body E has a slab shape and is only of the sources of the anomalies. It has magnetic susceptibility of 0.014 with depth of -154metres

(a)



(b)

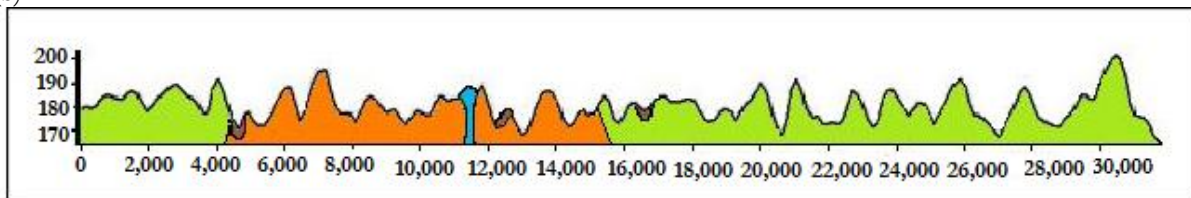
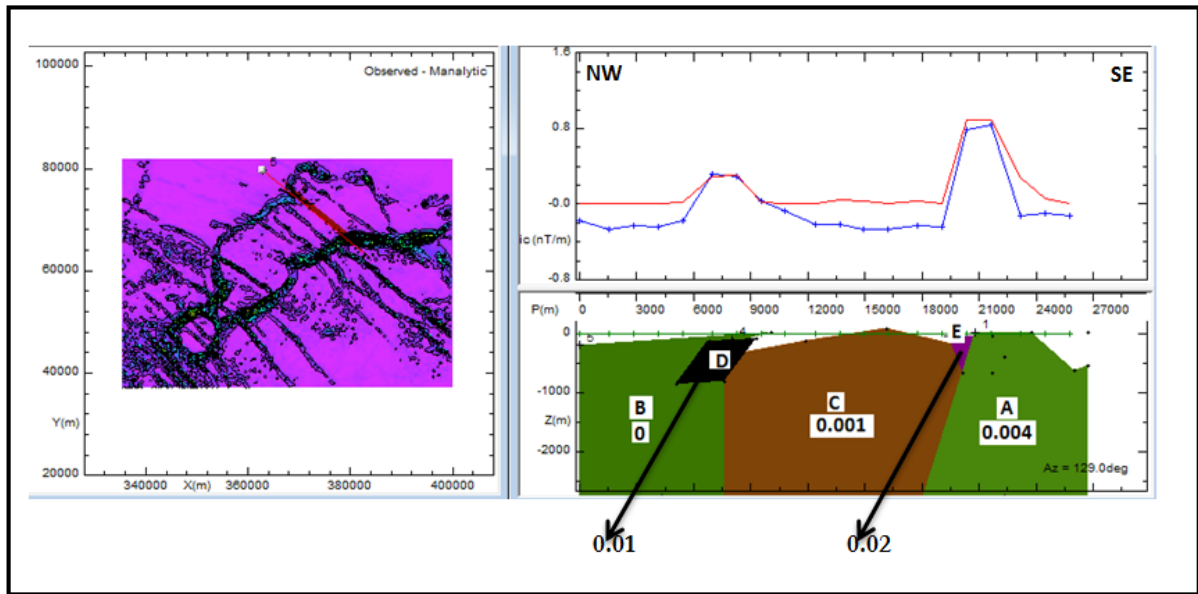


Figure 6.5: (a) Model of profile E-F; (b) Cross-section of profile E-F

- **Geological model of profile G-H**

Profile E-F was selected based on field work observation points that exist around much around it. This was done to validate field magnetic susceptibility result with magnetic susceptibility from Potent (Figure 6.6a and 6.6b). The body A and B has a slab shape representing the metasediments with magnetic susceptibility of 0.004 and 0 respectively. Body C represents the Singo granite with slab body shape and magnetic susceptibility of 0.001. Body D and E represent the anomalous bodies. D has dyke body shape with magnetic susceptibility of 0.01 with a depth of -110 meters. Body E has a slab shape and magnetic susceptibility of 0.02 with depth of -38metres.

(a)



(b)

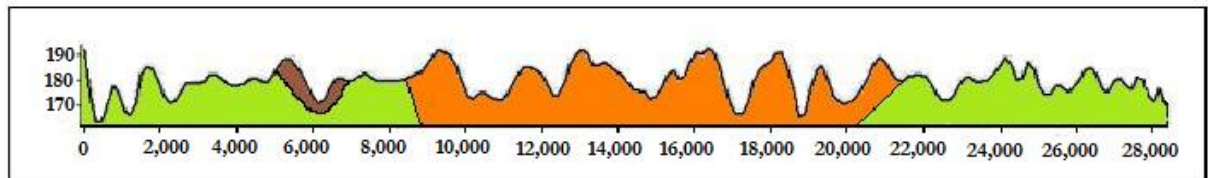


Figure 6.6: (a) Model of profile G-H; (b) Cross section of profile G-H

### Quantitative interpretation

The modelling of sources of the anomaly was carried out in order to get the quantitative interpretation of the anomaly. The conceptual models of the subsurface are created to see if the earth model is consistent with what has been observed. Magnetic models are coinciding with the geological cross section, which reflects the geology and how the rock is at the surface & subsurface including the cause of the magnetic anomaly.

The magnetic model along the profiles combined the observed and the calculated field with the conceptual geological model across the magnetic anomalies where the low magnetic anomaly expressions are related to the body of Singo granite and the metasediments. The magnetic susceptibility of these rocks varies from each other. The Singo granite has magnetic susceptibility of 0.003, 0.007 and 0.001 in the above profiles shown respectively. This might be due to the changes in mineral composition of the granite as a result of weathering. The dyke and the Xenoliths have positive and the highest magnetic susceptibility when compared to other rocks in the area. The constituents of the dyke makes it to have high magnetic susceptibility, while the Xenoliths which is an inclusion in the rock (Johnson & Williams, 1961). also contain some minerals rich in magnetite which also contribute to the high magnetic anomaly of the area. The depth of the dyke was estimated from the Euler deconvolution. The magnetic anomalies which occur at the contact between the Singo granite and the country rock might be due to dyke and the xenoliths.



## 7. DISCUSSION OF RESULTS AND CONCLUSION

The discussion of the results is based on the specific objectives outlined in chapter 1 for ease of reference.

### 7.1. Discussion

#### 7.1.1. To establish magnetic susceptibility contrast between granite and its surrounding rocks

The magnetic susceptibility measured along several walking traverses show that the values obtained in the sediments are highly variable i.e. 0.01, 0.05, 0.23 and 1.19. Similarly the measurements obtained in the areas covered by Singo granite have huge variations ranging from 0.03 to 5.72. In these area there was no noticeable feature contributing to the difference in magnetic susceptibility. However, it is inferred to be influenced by degree of weathering and therefore some measurements includes products of weathering. This explanation may be plausible to large extent considering that magnetic susceptibility measurements are confined within a depth of 3 metres. However, these measurements proved very useful as initial guess parameters for modelling in Potent.

During the fieldwork very few geological outcrops were encountered. This is because most of them are covered by thick undergrowth that hampered their mapping. Through use of the aeromagnetic anomaly map most of these areas that proved difficult to access during fieldwork were construed. The areas covered by the metasediments are reflected by relatively low magnetic anomaly that is laterally extensive (Figure. 6.2). The metasediments are products of deposition and metamorphism of quartzites, amphibolites, sandstones, siltstones, shale, phyllites and schists (Johnson & Williams, 1961), whose magnetic susceptibility is low. The trace of the Singo granite is clear on the geological map and expressed as high frequency magnetic source on the magnetic anomaly map. It was noted by (Johnson & Williams, 1961) that the boundary Singo granite and metasediments has xenoliths with tourmalised margin. It is inferred that this tourmaline that is a boron silicate mineral compounded with elements such as aluminium, iron, magnesium, sodium, lithium or potassium is the cause of the these high frequency magnetic sources. In addition, induration of hematite with its high iron content along the Singo granite and metasediment boundary (Johnson & Williams, 1961) also, contributes to these high frequency sources.

#### 7.1.2. To determine the depth to the source of magnetic anomaly

In this study, prior to modelling the surface and subsurface structures, the mapping of these structures was first carried out. The SRTM DEM including the ASTER images were used for this purpose which was noted that most lineaments follow the drainage pattern. On the aeromagnetic imagery it was noted that NW-SE linear features which were dykes are the dominant in the study area and they cut all the geological formations. Those located on the south western part of the study area are more dense (i.e. closely spaced) but short in size marking characteristic feature of tectonically active zones. In addition, the presence of echelon shaped deflections is an indication this area is tectonically active. The other NW-SE structures are long and more widely spaced indicating more evolved tectonic zones. The NE-SW is marked by only two features that cut across the NW-SE structures generally located within the alluvium near Lake Victoria. The E-W structures extend up to the NW-SE and do not cut across them and therefore no age relationship that can be drawn from them.

To further enhance structures from the aeromagnetic anomaly map several filtering techniques were applied i.e. analytical signal, tilt derivative, horizontal and vertical derivatives. On the analytical signal map,

apart from sharpening the boundary between the Singo granite and metasediments, the maps also shows enhanced structural features (NE-SW, NW-SE, E-W) indicating that these structures were covered by weathering material of low magnetic susceptibility that was filtered out by analytical signal processing. The strong magnetic susceptibility of these feature indicate that they are possibly buried dolerite dykes. In fact, the dolerite dykes on the geological map matches their location of the analytical signal indicating that this is not a mere coincidence.

On the tilt derivative the prominent and unique feature is the evidence of shearing effect on the NW-SE structures at the south western part of the study area that is not identified earlier in literature. The shearing has resulted into a large curvilinear structure near the southern margin of the Singo granite. Whereas the cause of the shearing is not known yet, its presence in an area that was construed to have short but closely spaced lineaments indicates a common geological phenomenon. A speculation of these could be magmatic intrusion of the granite, although a regional tectonic event cannot be ruled out. The horizontal derivative shows an increased number of NE-SW structures compared to other maps; these structures are clearly cut across by the NW-SE structures indicating that they are older. There is no identifiable contact between outline of Singo granite and the NE-SW structures to determine the age relationship. The vertical derivative proved useful for identifying two sub circular structures in the central part of the study area that seem somehow related to shearing.

3D Euler deconvolution was used to determine the depth of the magnetic sources associated with the anomalies displayed in the total magnetic intensity map and analytical map. The magnetic sources occur as either linear features or clustered. The linearised sources are oriented in either NW-SE or NE-SW, with NW-SE being widely distributed. Most of these magnetic sources are confined in the zone between 300-400 m but some are localised within shallow depths (100-200m). Another important characteristic is that the sub-parallel NE-SE is cut by the NW-SE structures, indicating a strong persistence of the NW-SE structures. Geologically, the NE-SW marks the Singo granite which majorly has no sources except along its outer margins and where it is cut through by the NW-SE structures. This indicates that the granite intrusion is much older than the faulting mechanism. The margin along the Singo granite possibly indicates lateritic material (alteration products i.e. tourmaline and hematite as noted in geology section) marking the contact between the Singo granite and the host rock. The clustered but isolated magnetic sources are rather deep seated (500m) and have a rather poorly defined E-W trend. The interpretation of these sources is not obvious at the moment from the limited information available.

### **7.1.3. To model the magnetic anomaly integrating surface and subsurface structures**

Whereas the 3D Euler deconvolution proved very useful for characterising the magnetic sources, it was found out the subsurface character of these magnetic anomalies were not fully construed. To overcome this shortcoming achieve Potent software was used. Three profiles were selected and magnetic susceptibility and depth determined through forward and inverse modelling techniques. It is clear from profile that the magnetic susceptibility of the metasediments is very low ranging from 0 to and 0.0005 whereas that of the granite is relatively slightly higher stable 0.003. These susceptibility values have the same order of magnitude for all the three profiles. Geologically, this means that the intrusion was rather confined within an existing fissure zone because on most cases the observed wedge observed in this is normally inverted i.e. narrowing as it approaches the surface. The main source of the magnetic anomaly at the boarders of the Singo granite is dyke and xenoliths.

#### **7.1.4. To establish the relationship between the magnetic anomaly, the geological structures and its associated mineralization**

The minerals present in the study area (gold, tin and tungsten) and are confined largely within the drainage system. The magnetic anomalies and geological structures proved very useful in this research because it enables the identification of the source of the magnetic anomaly. More information is needed to establish the relationship between the magnetic anomaly and the mineralization in the study area. Based on this study the magnetic anomaly modelled seems not to have relationship with mineralization. The mineral occurrence points fall on some of the dykes in the area (see Figure 5.10b) which could indicate that some correlation exist between the geological structures and the mineralization. Also, the identification of the shear zones and areas of localised tectonic activity in the south western part of the study area provides the first step towards target zones for gold i.e. gold occurrence in shear zone (Borg, et al., 1990). However, detailed geochemical mapping techniques are highly recommended.

#### **7.2. Conclusion**

The high magnetic anomalies along the margins of the Singo granite mark the xenoliths with tourmalised margin. A contribution of additional magnetic intensity comes from indurated hematite. Therefore, aeromagnetic technique can be used as a proxy for mapping of these anomalies. The NW-SE dykes are the dominant structures in the study area and they cut all the geological formations. Those located on the south western part of the study area are more dense (i.e. closely spaced) but short in size marking characteristic feature of tectonically active zones. In addition, the presence of echelon shaped deflections is an indication this area is tectonically active. The other NW-SE structures are long and more widely spaced indicating more evolved tectonic zones.

Subsurface characterisation of the anomaly shows depth result about 400meters which is relatively deep. Analytical signal map filters out weathering and enhances buried geological features (with detectable magnetic susceptibility); Tilt derivative was useful for mapping sheared zones. Horizontal derivative enhanced near surface structures while vertical derivative proved used for constraining sub-circular structures. The measurement of the magnetic susceptibility using a Kappa meter is not ideal for detailed magnetic mapping because it is confined within three (3) metres of probe, a zone highly affected by weathering. Therefore, the measurements mainly reflect indirectly degree of weathering rather than the magnetic content of the rock mass.

#### **7.3. Research Limitation**

The following limitations were encountered in the course of the research:

- Logistics problem was encountered during the field work; as a result enough field data was not obtained for the study.
- Measurement of magnetic susceptibility using a Kappa meter which is confined to three (3) metres of probe was not efficient for the detailed magnetic information needed for this study.

#### **7.4. Recommendation**

Based on limitations involved in this study, the following are recommended:

- Adequate and proper planning should be in place in case of more field work will be carried out in the study area in nearest future.
- Detailed geochemical mapping is recommended for more insight into the mineralization of the area.



## LIST OF REFERENCES

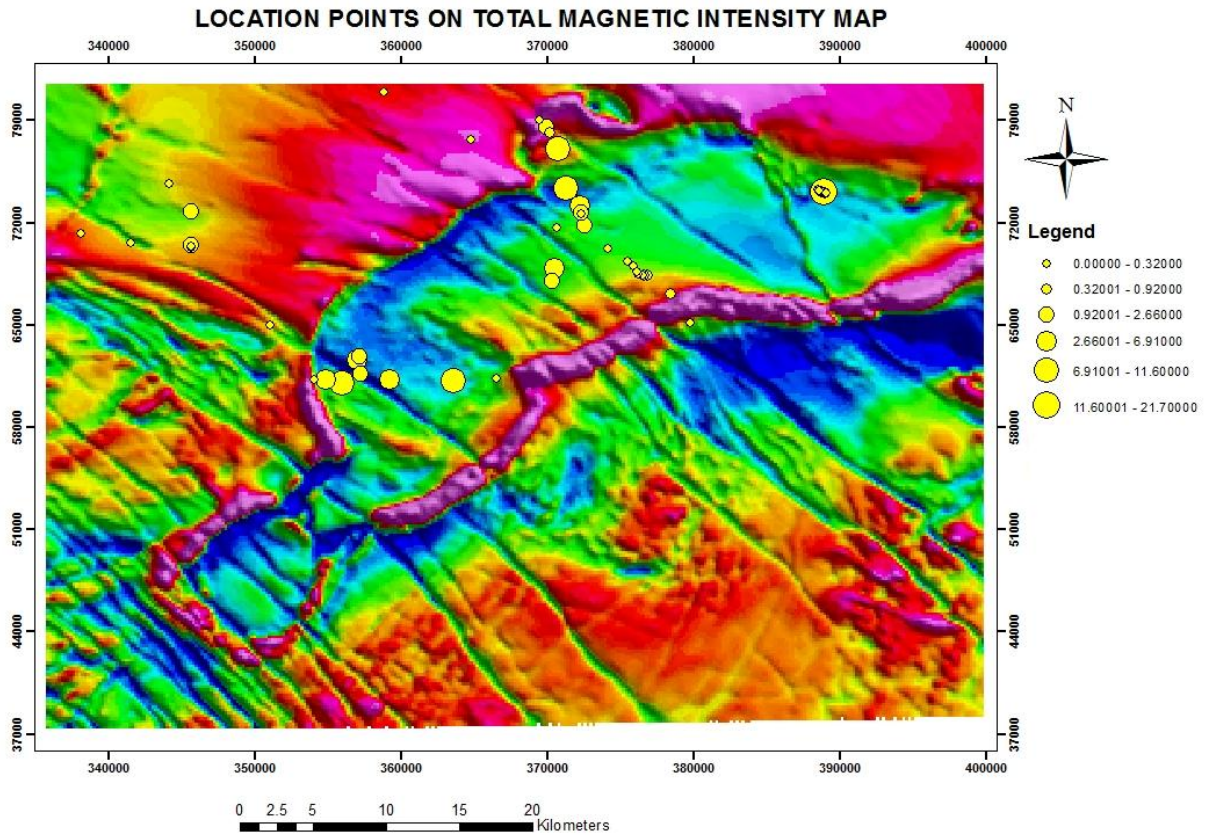
---

- Abarca, M. A. A. (2006). *Lineament Extraction from Digital Terrain Models: Case Study San Antonio del Sur Area, South-Eastern Cuba*, International Institute for Geo-information Science and Earth Observation, Enschede.
- Barbosa, V. C. F., Silva, J. B. C., & Medeiros, W. (1999). Stability analysis and improvement of structural index estimation in Euler deconvolution. *Geophysics*, 64, No. 1, 48-60.
- Borg, G., Lyatuu, D., & Rammlair, D. (1990). Genetic aspects of the Geita and Jubilee Reef Archean BIF-hosted gold deposits, Tanzania. *Geologische Rundschau*, 79(2), 355-371.
- Buchwaldt, R., Toulkeridis, T., Todt, W., & Ucakuwun, E. (2008). Crustal age domains in the Kibaran belt of SW-Uganda: Combined zircon geochronology and Sm-Nd isotopic investigation. *Journal of African Earth Sciences*, 51(1), 4-20.
- Clark, D. A. (1997). Magnetic petrophysics and magnetic petrology: aids to geological interpretation of magnetic surveys. *AGSO Journal of Australian Geology and Geophysics*, 17(2), 83-103.
- Clark, D. A. (1997). Magnetic petrophysics and magnetic petrology: aids to geological interpretation of magnetic surveys. [Journal]. *AGSO Journal of Australian Geology & Geophysics*, 17(2), 83-103.
- Clark, D. A., & Emerson, D. W. (1991). Notes on rock magnetization characteristics in applied geophysical studies. *Exploration Geophysics*, 22(3), 547-555.
- Gabert, G. (1990). Lithostratigraphic and tectonic setting of gold mineralization in the Archean cratons of Tanzania and Uganda, East Africa. *Precambrian Research*, 46(1-2), 59-69.
- Geosoft. (2010). Oasis Montaj Geosoft Manual, [www.geosoft.com](http://www.geosoft.com).
- Geosoft. (2010). Online Manuals, Tutorials and technical notes; Gravity & Magnetic Interpretation (Euler 3D).
- Gloaguen, R., Marpu, P. R., & Niemeier, I. (2007). Automatic extraction of faults and fractal analysis from remote sensing data. Nonlinear processes in Geophysics.
- Gunn, P. J., & Dentith, M. C. (1997). Magnetic responses associated with mineral deposits. [Journal]. *AGSO Journal of Australian Geology & Geophysics*, 17(2), 145-158.
- Hopgood, A. M. (1970). Structural Reorientation as Evidence of Basement Warping Associated with Rift Faulting in Uganda *Geological Society of America Bulletin*, 81, 3473-3480.
- Hunt, C. P., Moskowitz, B. M., & Banerjee, S. K. (1995). Magnetic properties of rocks and minerals. [American Geophysical Union]. 189-203.
- Jaques, A. L., Wellman, P., Whitaker, A., & Wyborn, D. (1997). High-resolution geophysics in modern geological mapping. *AGSO Journal of Australian Geology & Geophysics*, 17(2), 159-173.
- Johnson, R. J., & Williams, C. E. F. (1961). *Explanation of the Geology of sheet 59 (Kiboga)* (Vol. 7): Geological Survey Of Uganda, Authority of the Uganda Government.
- Kuttikul, P. (1995). Optimization of 3D Euler deconvolution for the interpretation of potential field data. *MSc Thesis*.
- Leggo, P. J. (1974). A geochronological study of the basement complex of Uganda. *Journal of the Geological Society*, 130, 263-276.
- Link, K., Koehn, D., Barth, M., Tiberindwa, J., Barifaijo, E., Aanyu, K., et al. (2010). Continuous cratonic crust between the Congo and Tanzania blocks in western Uganda. *International Journal of Earth Sciences*, 99(7), 1559-1573.
- Lunden, B., Wang, G., & Wester. K. (2001). A GIS based analysis of data from Landsat TM, airborne geophysical measurements, and digital maps for geological remote sensing in the Stockholm region, Sweden *international Journal of Remote Sensing*, 22, 517-532.
- McConnel, R. B. (1972). Geological Development of the Rift Systems of Eastern Africa. *Geological Society of America Bulletin*, 83, 2549-2572.
- Nagudi, B., Koeberl, C., & Kurat, G. (2003). Petrography and geochemistry of the Singo granite, Uganda, and implications for its origin. *Journal of African Earth Sciences* 36(2003), 73-87.

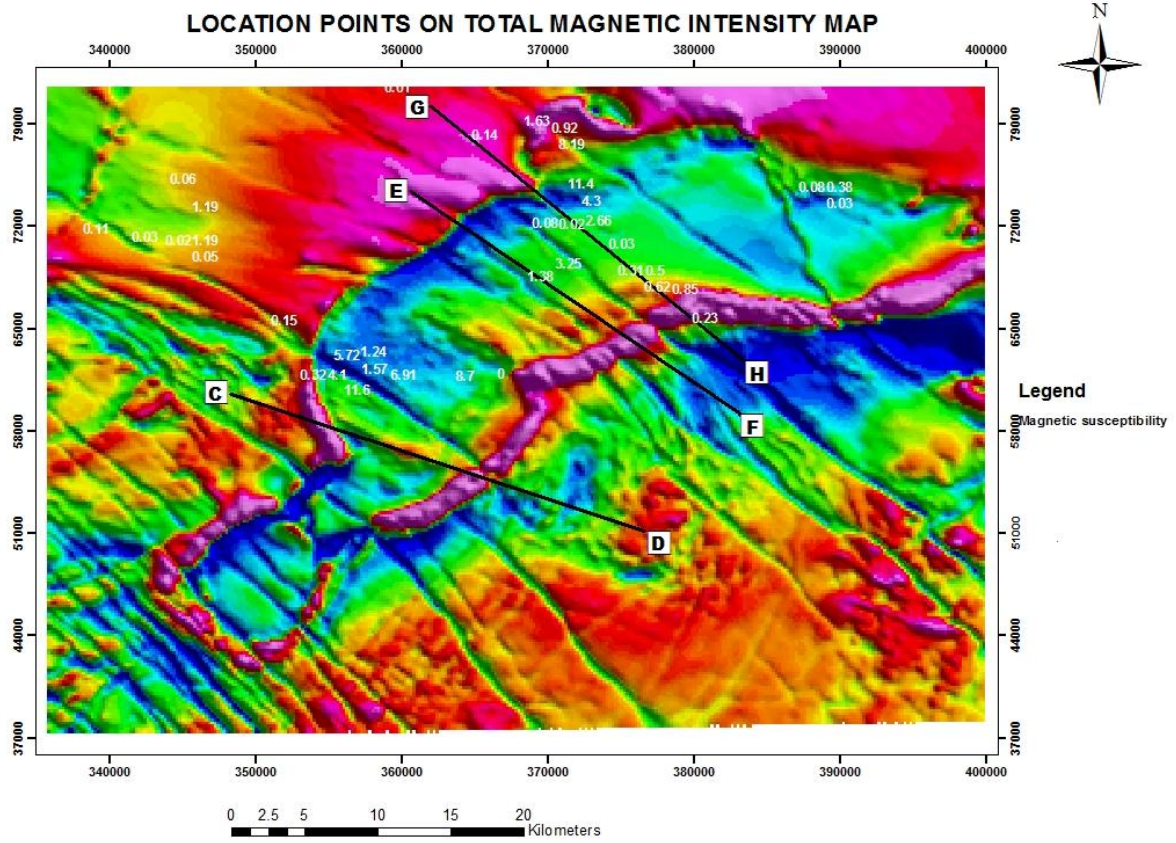
- Nyakairu, W. A., & Koeberl, C. (2001). Mineralogical and chemical composition and distribution of rare earth elements in clay-rich sediments from central Uganda. *Geochemical Journal*, 35, 13-28.
- Nyakairu, W. A. G., Christian, K., & Kurzweil, H. (2001). The Buwambo kaolin deposit in central Uganda: Mineralogical and chemical composition. *Geochemical Journal*, 35, 245 to 256.
- OMI. (2006). Opportunities for mining investors in Uganda: The Republic of Uganda, <http://www.magnusresources.com/docs/media/UgandaMining2006.pdf>.
- Potent. (2010). Geophysical software solutions manual, [www.geoss.com.au](http://www.geoss.com.au).
- Reid, A. B., Allsop, J. M., Granser, H., Millet A, J., & Somerton, I. W. (1990). Magnetic interpretation in three dimensions using Euler Deconvolution. *Geophysics*, 55, 80-90.
- Teichrieb, V., & Kelner, J. (2007). Enhancement of Radar Based DEMs Using 3D Techniques. [Geoscience & Remote sensing symposium]. *IEEE International*, 4902-4905.
- Thompson, D. T. (1982). EULDPH: A new technique for making computer-assisted depth estimates from magnetic data. *Geophysics*, 47, 31-37.
- Thurmond, A. K., Abdelsalam, M. G., & Thurmond, J. B. (2006). Optical-radar-DEM remote sensing data integration for geological mapping in the Afar Depression, Ethiopia. *Journal of African Earth Sciences*, 44(2), 119-134.
- Verduzco, B., Fairhead, J. D., Green, C. M., & Mackenzie, C. (2004). New insights into magnetic derivatives for structural mapping. *THE LEADING EDGE*, 116-119.
- Williams, N. C. (2009). Mass and magnetic properties for 3D geological and geophysical modelling of the southern Agnew-Wiluna Gneiss Belt and Leinster nickel deposits, Western Australia. *Australian journal of earth sciences*, 56, 1111-1142.
- Woldai, T. (2010). Note on geology of Uganda.

APPENDIX -01

Field location points displayed on total magnetic intensity map.



APPENDIX 02



## APPENDIX - 03

List of field magnetic susceptibility values

<b>NO</b>	<b>x- coordinate</b>	<b>y- coordinate</b>	<b>z- coordinate</b>	<b>Magnetic susceptibility value</b>	<b>lithology</b>	<b>lithology property</b>
1	338090	71202	1265	0.07	quartzites	unweathered
2	341527	70629	1264	0.04	quartzites	unweathered
3	345626	70400	1365	0.02	metasediment	unweathered
4	345626	70406	1370	0.03	metasediment	unweathered
5	345624	70321	1358	0.05	quartzites	unweathered
6	345641	72737	1392	0.06	quartzites	unweathered
7	351061	64991	1231	0.34	metasediment	unweathered
8	355983	61000	1266	12.65	granite	unweathered
9	356990	62597	1290	6.62	granite	unweathered
10	357141	62836	1308	1.34	granite	unweathered
11	363570	61155	1247	7.53	granite	unweathered
12	370303	67979	1248	1.19	granite	unweathered
13	370450	68870	1248	3.48	granite	unweathered
14	370647	71596	1216	0.06	quartz-sericite	unweathered
15	371298	74335	1169	11.86	granite	unweathered
16	372324	72664	1225	3.49	quartzites	unweathered
17	372351	72629	1230	2.182	quartzites	unweathered
18	372562	71773	1234	2.19	granites	unweathered
19	374140	70179	1259	0.03	quartz sericite	unweathered
20	375454	69309	1255	0.01	quartz-sericite	unweathered
21	375926	68881	1266	0.05	granite	unweathered
22	68586	376115	1268	0.01	granite	unweathered
23	376238	68431	1268	0.12	granite	unweathered
24	376517	68373	1269	0.15	granite	unweathered
25	376558	68360	1270	0.34	granite	unweathered
26	376629	68355	1274	0.13	granite	unweathered
27	378457	67081	1236	1.24	metasediment	unweathered
28	65143	379799	1245	0.23	metasediment	unweathered
29	77661	364760	1196	0.12	metasediment	unweathered
30	369486	79019	1152	0.08	metasediment	unweathered
31	369941	78573	1164	1.73	granite	unweathered
32	370695	77010	1168	8.74	granite	unweathered
33	358833	80926	1157	0.01	quartzites	unweathered
34	388632	74174	1318	0.02	quartzites	unweathered
35	388731	74117	1317	0.24	granite	unweathered
36	388894	74115	1326	0.12	granite	unweathered
37	388909	74104	1328	27.82	doleritic dyke	unweathered
38	389006	74035	1337	0.14	granite	unweathered
39	389034	74035	1340	0.02	granite	unweathered
40	388894	74115	1326	0.14	granite	unweathered

<b>N0</b>	<b>x- coordinate</b>	<b>y- coordinate</b>	<b>z- coordinate</b>	<b>Magnetic susceptibility values</b>	<b>lithology</b>	<b>lithology property</b>
41	388894	74115	1326	0.12	granite	unweathered
42	370647	71596	1216	0.06	quartzites	unweathered
43	344130	74650	1345	0.06	metasediment	unweathered
44	358833	80926	1157	0.01	quartzite	unweathered
45	354032	61248	1294	0.16	sandstone	weathered
46	354831	61221	1296	2.73	granite	weathered
47	357198	61598	1287	1.66	granite	weathered
48	359201	61209	1254	4.59	granite	weathered
49	366487	61283	1224	11.21	granite	weathered
50	370647	71596	1216	0.06	quartz-sericite	weathered
51	372220	733108	1209	4.3	granite	weathered
52	376825	68340	1263	0.43	metasediment	weathered
53	370194	78110	1157	4.14	granite	weathered
54	388570	74183	1315	0.08	quartzite	weathered
55	388522	74223	1313	0.08	granite	weathered

